Preliminary design and analysis of fuel systems for box-wing aircraft

R. Piet

Technische Universiteit Delft

TU Delft Delft University of Technology

Challenge the future

Preliminary design and analysis of fuel systems for box-wing aircraft

by

R. Piet

in partial fulfillment of the requirements for the degree of

Master of Science
in Flight Performance and Propulsion

at the Delft University of Technology,
to be defended publicly on Friday February 11, 2022 at 01:00 PM.

Supervisor:	Dr. ir. G. La Rocca	
Thesis committee:	Dr. F. Oliviero,	TU Delft
	Ir. P. C. Roling,	TU Delft
	C. Varriale MSc,	TU Delft

TU Delft Delft University of Technology

Summary

With an expected annual increase in traffic of 5%, the aviation industry faces the challenge of reducing carbon dioxide emissions such that the targets set by regulatory bodies can be met. It can be argued that the evolution of conventional aircraft will not be sufficient to meet these targets, so revolution is required. Project PARSIFAL aims to provide such revolution by introducing a box wing aircraft as an alternative configuration. The objective of this thesis is to contribute to project PARSIFAL by questioning if, given the box wing aircraft, the opportunity of splitting the fuel over two large tanks in front and behind the aircraft CG can be exploited to achieve an improved active control of the CG, thereby reducing trim drag and improving the loading flexibility.

This thesis makes use of two in-house tools developed at TU Delft: the Multi-Model Generator (MMG) and the Performance, Handling Qualities and Load Analysis Toolbox (PHALANX). The former is capable of generating preliminary designs from a set of top-level requirements, including the box wing aircraft. The latter is a non-linear flight dynamics analysis tool, evaluating the aircraft performance characteristics and assessing the aircraft stability. The MMG has been extended with a fuel system design module capable of creating and assessing preliminary fuel systems, and a simulation module simulating a cruise-only mission with said fuel system. The design module uses the aircraft geometry model created by the MMG, and a user-defined input file to generate a fuel system geometry model. The geometry model is used to estimate the fuel system mass and CG. Afterwards, the relevant databases in PHALANX are updated, and, given the flight condition, used to find the the instantaneous fuel flow. A mission is then simulated by setting the starting fuel distribution, updating the fuel mass and CG in a simple time-stepping loop until all fuel is consumed. The user can opt for a pre-set burn sequence to investigate the flight envelope of the design, or use a active CG control algorithm in hopes of finding the optimal fuel consumption.

In order to significantly speed up the simulation, the PHALANX analysis can be replaced by a surrogate model. Using this surrogate model, however, omits any aerodynamic and structural effects from the results. While it is assumed that no aerodynamic effects occur when only the fuel system design is changed, changing any of the aircraft design parameters will cause aerodynamic effects and demand changes in the structure of the aircraft.

Results indicate that it is advisable to use the connecting element between the front wing and rear wing to connect the fuel tanks in the wings, saving up to 6% system weight compared to designs that use the fuselage to connect the tanks. Adding a forward trim tank adds roughly 8% to the system weight, while increasing the stable, usable CG range over the course of a mission by 12-15%, and increasing the flight envelope by up to 3%MAC. Compared to a conventional aircraft, however, the effect of adding a forward trim tank is minor. Hence it is unclear if the added system complexity of a forward trim tank outweighs the operational benefits of the increased CG range. In any case, simulations indicate an insignificant fuel save of 0.2kg for the trim tank.

Finally, at the start of the flight, the effects of aircraft parameters on the fuel system and the aircraft's balance are mostly dominated by the interaction between the rotor burst zone and the rear wing tank. At the start of the flight, the change in rear wing tank size due to the shift of the rotor burst zone dominated any changes in the CG caused by the system weight or fuel CG shift. At the end of the flight, the effect of the fuel system on the CG is minor compared to the effects of structural changes warranted by changing the engine position, sweep angles, or spar locations.

Preface

I find myself writing this preface in the middle of the night, looking to do something a little less intensive than some of the other tasks that should finalise this thesis. It feels like an eternity since the day I started working on it. Actually, it really has been a long time - the circumstances under which this work has come to be certainly have not been kind. While this work was in progress, the world was taken hold of by a virus that to this day limits the freedom of many people around the world.
Another foul disease, however, unironically takes the cake by taking away my mother in an untimely fashion. Is such a passing ever timely, though? We often ride the highs of life and tend to forget what is down below. In any case, it is in these moments that she would often find a way to shine a little light, and the world would be better for it. How I would have wished for her to see this.
I am thankful for all the people that have chosen to stay with me, and that have supported me throughout. They might not know it, for their contributions may be small. But I have learned along the way that even the smallest of contributions can lead to many good things. To my dad, brother, their loved ones, and my masters, you know your contributions have been anything but small, and I hope you choose to stay a little longer.
Finally, I am eternally grateful for my supervisor, Dr. Ir. Gianfranco la Rocca. There have been times where I wished I had made more efforts to let you know what was going on, in my work, or in my mind. And despite my own best efforts to sabotage myself, you too chose to stay with me. I will never forget your understanding of the situation I found myself in, and how important it was to you that I was well. I hope many other students will find such support in their lives.

R. Piet
Delft, December 2021

Contents

List of Figures

List of Tables

1

Introduction

With an expected annual increase of 5%, the aviation industry faces the challenge of reducing carbon dioxide missions such that the targets set by regulatory bodies can be met [9]. Emission targets like those set in [10], where carbon dioxide emissions should be reduced by 75% per passenger per kilometre by 2050, seem hardly attainable with incremental improvements to conventional tube and wing layouts. Indeed, if the evolution of contemporary aircraft is insufficient, revolution may be required. Unconventional configurations, however, often cannot match the level of maturity of conventional layouts. Unlocking their potential may prove to be the revolutionary step required to achieve emission targets.
When considering unconventional wing systems, the box wing stands out since theoretically it has the lowest induced drag [11]. The box wing is characterised by two lifting wings, with the tips connected by a (vertical) connecting element. When projected on the longitudinal axis, the configuration has a rectangular shape, and is therefore referred to as a box wing. Often times, box wing designs stagger the upper and lower wing, where the lower wing is in front and swept back, while the upper rear wing is swept forward.
Over the years, the box wing has garnered the attention of several researchers. In the 1970s, Lange *et al.* [1] performed a feasibility study on a long-range box wing, eventually deeming the design infeasible due to flutter concerns. More recently, Schiktanz and Scholz [2] and Andrews and Perez [3] presented designs for short to medium range box wing aircraft. Both acknowledged the potential aerodynamic benefits of the box wing and raised concerns regarding the allocation of fuel. Indeed, dividing a reference cantilever wing into two seperate wings with half the chord and similar taper and aspect ratio results in a lifting surface with half the volume of its cantilever counterpart. Cipolla *et al.* [12] circumvent the fuel allocation problem by introducing a box wing with comparatively low range and high payload, which increases the total lift requirement and alleviates the fuel allocation problem. Additionally, it has been recognized that the box wing configuration can be exploited from an operational viewpoint, specifically in the areas of safety, passenger comfort, turn-around time, and boarding times [4].

Advantages for box wing fuel systems may come in their inherent capability to control the Centre of Gravity (CG). Conventional aircraft store the bulk of their fuel in the main wing, and are sometimes equipped with a trim tank in the horizontal stabiliser. By moving fuel to and from the trim tank, the CG of the aircraft can actively be controlled in an attempt to reduce the trim drag [5]. In this case, one makes a trade-off between the added system complexity and weight that a trim tank brings, and the reduction in trim drag it offers. Box wing aircraft, on the other hand, are inherently capable of controlling the CG by moving fuel between the front and rear wing - a trade-off need not be made. Additionally, CG control can improve the operational flexibility of the aircraft in terms of loading.
On the other hand, it was already alluded to that the available volume in the wings is greatly reduced for a box wing aircraft, leading to fuel allocations problems. Moreover, splitting the fuel volume into two (equally) large volumes placed relatively far from the aircraft CG may inadvertently lead to dangerous situations in case of system malfunctions. If malfunctions lead to an uncontrollable aircraft or if the fuel system is critical in keeping the CG within the flight envelope, additional redundancy may be

required.
With the ostensible need for revolutionary ideas and the advantages that the box wing seems to offer, Project PARSIFAL (Prandtlplane ARchitecture for the Sustainable Improvement of Future AirpLanes) has set out to quantify its expected advantages. This thesis aims to contribute to project PARSIFAL by providing insight in 1) how the box wing aircraft configuration can be exploited to improve aircraft performance, 2) the effects of fuel system design choices on aircraft performance, and 3) the effects of aircraft design parameters on the fuel system. In all, the lead question is if, given the box wing aircraft, the opportunity of splitting the fuel over two (equally) large tanks in front and behind the aircraft CG can be exploited to achieve an improved active control of the CG, thereby reducing trim drag and improving the loading flexibility.
The remainder of this paper follows a conventional layout comprised of an investigation of literature, methodology, results, discussion and conclusions. The literature section is predominantly aimed at investigating how fuel systems impact aircraft performance.

2

Fuel system design and performance

In the early stages of aviation, fuel systems were simple systems. Often times fuel tanks were gravity filled, engines were gravity fed, and the fuel level was measured using simple flotation devices. Much has changed since these early days. Increased fuel volume requirements, increased fuel flow demands and challenging operating conditions mandate much more complex fuel systems. In a similar vein, safety requirements have become more strict and may required additional functions such as fuel transfer, jettison, and inerting.

While it is true that fuel systems have become increasingly complex, simple fuel systems have not ceased to exist. In fact, one would still expect the fuel system of a light aircraft to be relatively simple, possibly consisting of a single gravity-filled tank. On the other side of the spectrum are modern military jets with complex arrangements of fuel tanks, pressurised so they can operate at high altitudes, with systems in place that allow for quick shifts in the CG. Somewhere in between these levels of complexities one finds civil aircraft like the A320 and B777. Their fuel systems are comprised of 2-3 tanks, are not pressurised, and some times feature active CG control, though shifts in the CG may be slow.

According to EASA, CS-25 [13], the core function of a fuel system is to ensure fuel flow at a specified rate and pressure for proper engine functioning. This must be achieved at any flight condition for which the aircraft is certified, which could include negative-G conditions. It goes without saying that to provide fuel flow, the tanks must be able to hold sufficient fuel to complete the intended mission.

This thesis defines the fuel system as aircraft components aimed at handling fuel from the refuel source to the delivery of fuel to the engines of the aircraft [5]. It is scoped to only deal with the preliminary design of the fuel system, where the fuel system is limited to the design of the fuel tanks, fuel lines, pumps, and valves, using only state-of-the-art technologies (as mentioned in [4]). Any system beyond the engine shutoff valve is not modelled. Also, the fuel inerting system, quantity gauging, and venting systems are not modelled. The focus also lies on civil aircraft, meaning that the thesis will forego the modeling of external tanks, tank pressurisation, and quick fuel transfer to allow for quick changes in the CG to deal with changes in the centre of pressure resulting from subsonic-supersonic operations. Aside from the system itself, this thesis also investigates the effect of the fuel within the system, particularly focusing on how CG control can be employed to improve aircraft trim drag and loading flexibility.

This chapter first explores how other authors have dealt with fuel system design in preliminary design studies. Next, it is investigated what is meant by fuel system performance. Finally, fuel systems are considered in the context of box wing aircraft, noting any opportunities and challenges in the fuel system design.

2.1. Fuel system design

According to Langton *et al.* [5], it is important to take the fuel system into account at an early stage in the design process. The reason being that retrofitting a fuel system is time consuming due to the amount of space the system occupies. Additionally, the fuel constitutes a large portion of the aircraft weight and is a large contributor to the balance of the aircraft. Consequently, one will notice that many preliminary studies for aircraft include the tank volume and trim constraints in their optimisations

[14] [15] [16] [17] [2] [12]. Many studies that included a tank volume constraint in box wing aircraft optimisation studies found tank volume to be an active constraint. An explanation for this is provided in [2], where it is assumed that the reference wing is divided into two separate wings with half the chord, which in turn halves the thickness of the two wings. If the taper is also kept the same for both wings, and the aspect ratio of a single box wing is twice that of the reference wing, the result is that the total wing volume of the box wing aircraft is half the volume of the reference cantilever wing aircraft.
Regarding stability, one will find that the fuel is the component whose shift in position has the largest effect on the CG [18]. To add to this, fuel tanks are often not located at the CG, so during the mission the CG will shift as a result of fuel being used. Transferring fuel from one tank to another has similar effects. Some manufacturers (notably Airbus) deliberately place fuel tanks far from the CG to increase the fuel tank's moment in a attempt to exert control over the CG by transferring fuel from and to this tank.
The fuel allocation and stability design problems are mostly concerned with the fuel and applicable at an early stage of the design. At a systems component level, the designer is faced with the problem that the different functions of the fuel system can be fulfilled by different components and/or concepts. For example, fuel can be transferred using either variable frequency pumps, constant frequency pumps, or jet pumps. After choosing the pumps (i.e. the components), one also has the choice of using the siphoning concept or distributed pumps concept to transfer fuel.
Studies often make use of morphological matrices [19] [20] to map the possibilities in their design task. By adding a performance assessment module for each combination in the morphological matrix, one creates a system capable of creating and assessing designs, essentially creating a quantified morphological matrix. Theoretically, one could pick the best design from this matrix, if not for the computational cost it often requires. Replacing the exhaustive approach by an optimisation algorithm has been shown to reduce the computational effort [20] [21]. In [22], [23], [24], [6], and [25] such an optimisation framework is presented for several aircraft subsystems, where only [6] disregards the fuel system.

2.2. Fuel system performance

There are many aspects in which a fuel system can perform well and often times researchers either specifically focus on one aspect, or generalise several aspects in order to fit the model in a larger framework. In case of the latter, efforts are usually aimed towards sizing a set of systems for the aircraft. When the fuel system is considered in such a sizing tool, models with limited fidelity are often used. In [24], the fuel system weight and power off-take are estimated using the maximum fuel weight and maximum takeoff weight, respectively. In [25] the electrical sizing of the fuel system is approximated using a more detailed model of the fuel system, where the system topology is used to make an estimate. Boggero [23] go one step beyond and define and size the fuel lines and boost pumps for their fuel system to find the weight and shaft power off-take. Finally, Rajaram *et al.* [6] proposed a model with which the impact of any aircraft system can be captured, taking into account the weight, zero-lift drag, shaft power off-take, and bleed air off-take.
When the fuel system is considered in more detail, it becomes evident that system weight and power off-take are not the only factors defining fuel system performance. One can also consider the fuel system's transfer capability to be a performance indicator. It has already been noted that this thesis will not consider the rate at which the CG can be moved, but it will consider the range over which the CG can be moved, where a larger range can lead to increased operation flexibility. Moreover, it has been shown that by actively controlling the CG to a more desirable position in terms of trim, fuel consumption can be reduced by up to 2% [26]. Langton *et al.* [5], on the other hand, maintain that the implementation of tanks and equipment for active CG control may not always outweigh the operational benefit for civil airliners. Regarding operational flexibility, it has already been mentioned that the fuel tanks should hold sufficient fuel for the envisioned mission, effectively creating a minimum fuel capacity. Increasing the tank size, however, also increases the operational flexibility.
The reliability of the fuel system may also be of concern to the designer. Some designers choose to add a reliability target for their design [27]. In any case, any performance can essentially be nullified when the fuel system does not meet reliability and/or safety requirements and becomes inadmissible for certification. In a similar fashion, poor thermal endurance can nullify gains made in the fuel system

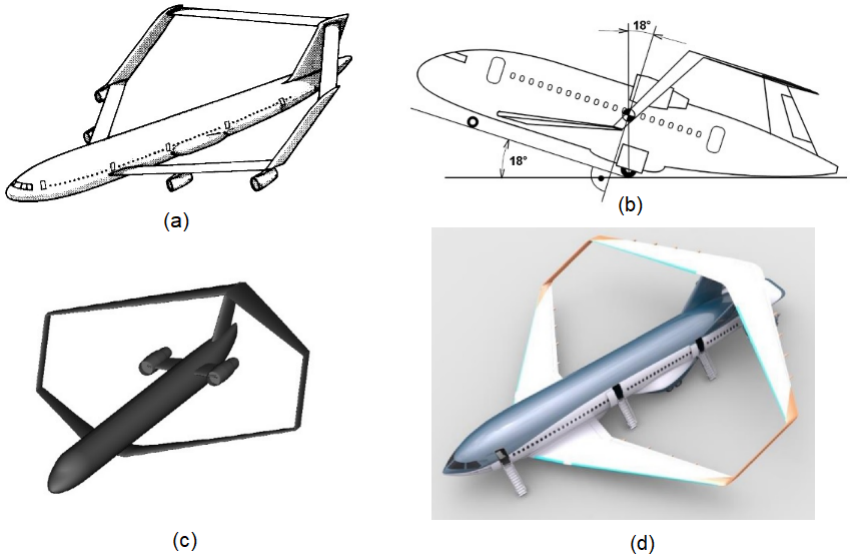

Figure 2.1: Box wing designs from [1], [2], [3], and [4], respectively.

performance by adding a requirement for tank inerting. Indeed, aluminum wings are exempt from inerting requirements, as it is assumed that surrounding air sufficiently cools the fuel to avoid flammable circumstances. Composite wings, however, have reduced cooling interaction with the surrounding air and are therefore not exempt from inerting requirements [28] [29] [13]. While is it the ambition of the PARSIFAL project to use composite wings, this thesis is scoped to not deal with inerting systems.

2.3. Box wing fuel systems

When considering a box wing aircraft from a fuel system design perspective, it is important to have a clear understanding of the general layout of box wing aircraft. For reference, four designs are presented in Fig. 2.1, where the bottom right design is an artist's impression of the PARSIFAL baseline concept, i.e. the aircraft this thesis focuses on. Common traits found among the box wing aircraft include staggering of the wings, and a significant height difference between the wings. In all designs, the front wing is the lower wing and is swept back, while the rear wing is higher up, connected to the vertical tail(s) and swept forward. The engines are either mounted on the fuselage or on the front wing, though one should not discount the possibility of the engine being mounted on the rear wing.

The box wing configuration creates a number of opportunities while simultaneously posing challenges to the designer - they are summarised in Table 2.1. The first challenge relates to the allocation of the mission fuel. By splitting the main wing into two separate wings, the combined available volume is essentially halved. Cipolla *et al.* [12], however, have shown that by reducing the intended range and increasing the payload it is still possible to define a box wing aircraft with reasonable top level requirements and sufficient space to allocate the mission fuel.
Second, since the fuel is distributed into two wings far from the CG, burning said fuel can cause a significant change in the CG. Figure 2.2 shows how conventional aircraft use trim tanks in the empennage to create meaningful pitching moments to decrease trim drag. As fuel is transferred to and from the trim tank, the CG is kept within a control band which represent a CG range wherein trim drag is minimised. This is referred to as active CG control, and the concept has been shown to reduce fuel consumption by up to 2% [26]. Active CG control may also be used to increase the operational flexibility of the aircraft in terms of payload, as shifting the CG using fuel can compensate any changes in payload CG. Jemitola and Fielding [30] note that to trim their box wing aircraft, elevator deflections of 3.10° and -5.13° for the front and rear wing, respectively, were required. They suggest that these elevator deflections could reduce the advantages of the box wing, and that active CG control could help unlock the aircraft's potential. The key point here is that a box wing aircraft is naturally equipped

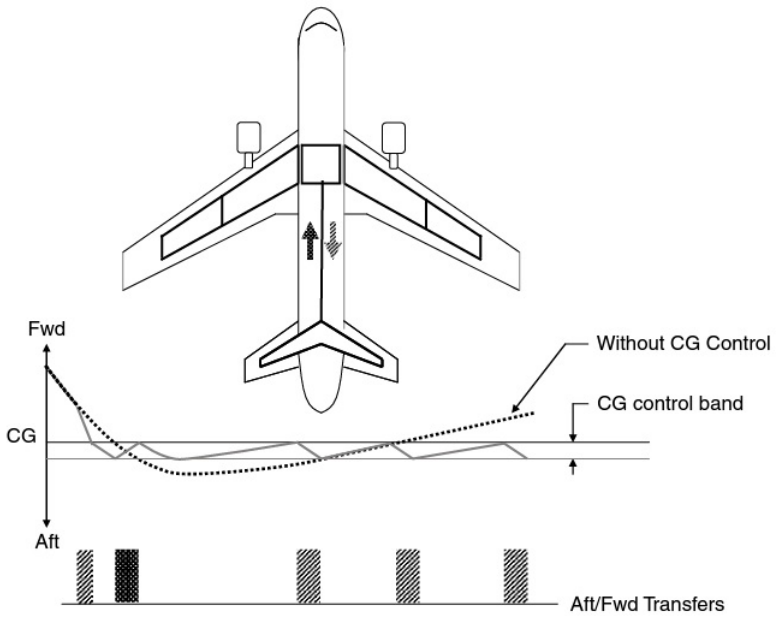

Figure 2.2: Active cg control principle [5]

with active CG control capability, due to the staggering of the wings. Even more so, the rear wing may comprise up to 30% of the fuel capacity, where trim tanks for conventional aircraft regularly comprise 3% of the fuel capacity. That said, it may be possible to equip a box wing aircraft with an additional trim tank in the forward part of the aircraft. For this, a trade-off should be made, as is the case for trim tanks in the empennage of conventional aircraft.

While the staggering of the wings creates a 'free' active CG control system, it also poses some safety concerns. It is easy to imagine that when a transfer pump or valve fails, it might no longer be possible to transfer fuel from a tank, essentially trapping the fuel inside. Such trapped fuel may inadvertently cause large pitching moments that can no longer be counteracted, jeopardising the aircraft's stability and controllability. In case of the box wing aircraft, this can be especially problematic since large amounts of fuel could be trapped far from the CG due to the staggering of the wings. Such extremes should be explored should be explored in the preliminary design phase where it may still be possible to alter the design to avoid such scenarios. An increased level of redundancy is required in cases where the aircraft's controllability and stability are compromised when parts of the transfer system are inoperative. Implementing components in parallel (e.g. doubly implementing cross transfer valves) may provide such redundancy and lower the probability of catastrophic events to an acceptable level.
Another factor to consider is the height difference between the front and rear wing. The transfer pumps that provide flow from the front to the rear wing must overcome additional pressure due to the height difference. Boost pumps placed in the front wing face similar issues if the engines are not placed underneath the front wing. Even more so, during landing, variable frequency motor-driven boost pumps will have to deal with additional height differences caused by a nose-down attitude, in combination with low frequency running due to low thrust settings. On the other hand, such height differences ease opportunities such as gravity transfer from the rear wing to the front wing, and downsizing of override boost pumps in the rear wing.

Table 2.1: Opportunities and challenges of a box wing fuel system.

Feature	Opportunity	Challenge
Two lifting surfaces with connected tips	-	Wing volume is halved, making the allocation of mission fuel difficult
Staggered wings	Inherent active CG control, possibly leading to reduced fuel consumption and increased operational flexibility	Trapped fuel may cause significant pitching moments
Height between wings	Reduced pump size in the rear wing	Increased pump size in front wing

3

Methodology

This thesis makes use of two in-house tools developed at TU Delft: the Multi-Model Generator (MMG) [31] and the Performance, Handling Qualities and Load Analysis Toolbox (PHALANX) [32]. The former is a Knowledge-Based Engineering (KBE) [33] tool capable of generating preliminary designs from a set of top-level requirements for many aircraft, including the box wing aircraft. The latter is a non-linear flight dynamics analysis tool, which can be used to evaluate aircraft performance characteristics and assess static and dynamic stability.
For this thesis the MMG has been extended with a fuel system design module capable of creating and assessing preliminary fuel systems, and a simulation module simulating a cruise-only mission with said fuel system. The MMG is an aircraft type agnostic tool, meaning that is is capable of generating any type of aircraft. Likewise, the fuel system design module (for brevity's sake, from here on the module) creates fuel systems regardless of the type of aircraft, and the design can be adapted for each aircraft. In short, the module uses the aircraft geometry created by the MMG and a user-defined .json-file to generate a fuel system geometry model using the Parapy software package [34]. The geometry model is used to estimate the fuel (system) mass and CG, which are used to update the mass and inertia database fed to PHALANX. For a given flight condition, the fuel flow can then be extracted from the resulting trim condition computed by PHALANX. A mission can be simulated by setting a starting fuel distribution, updating the fuel mass and CG in a simple time-stepping loop until all fuel is consumed. The fuel system performance can then be assessed by investigating in-flight parameters, e.g. the range, and CG position.
This chapter starts by discussing how fuel system performance is defined. Next, the workflow of the module is discussed in greater detail, initially focusing on the information exchange between the MMG, PHALANX, and the module. Next, the internal methods of the fuel system model are expanded upon, taking a detailed look at the design module and the simulation module. The chapter ends with the design of experiments. In this chapter, the focus is primarily on box wing aircraft, as most examples will feature box wing aircraft. Nevertheless, the concepts also apply to conventional layouts.

3.1. Fuel system performance

Earlier in section 2.2 it was noted that fuel system performance can take on many shapes and forms. Fuel burn, operational flexibility, reliability, and thermal endurance are all indicative of how well a system performs. First off, the thermal endurance of the aircraft is outside the scope of this thesis, while it also requires information on a number of thermal management systems which are simply not available to the author. For more information on how to use the fuel system topology to increase the thermal endurance of the aircraft, the reader is referred to [28] and [29]. Second, this thesis will not deal with the reliability as the author lacks data on the reliability of the components used in the fuel system design. The reader is referred to [27] for a method to estimate the reliability should this data become available. The two performance indicators this thesis will deal with are the total fuel burn over a cruise-only mission, and the operational flexibility.
In the preliminary design stage, research often relies on statistics to estimate performance metrics -

they are computationally cheap and therefore well suited to perform many design evaluations. However, their statistics are often derived from conventional layouts, hence they may restrict the exploration of novelties within the design. Numerous authors have therefore expressed the importance of using physics-based estimation methods [20] [35] [36]. While such statistical approximations can result in accurate estimates, they often have a limited number of inputs, e.g. relying on only the number of tanks and the wing length to estimate the weight of the fuel system. The consequence is that such methods are insensitive to small changes in the (fuel system) design.
Admittedly, the choice for using the MMG and PHALANX has been largely influenced by the ease with which the tools were available. That does not, however, mean that they come without any merit. In fact, the KBE approach in the MMG, or rather using a KBE approach in general, means that there is access to the geometries of many aircraft, including the box wing aircraft. This will increase the possibility of using physics-based analysis, as a greater level of detail can be achieved. Additionally, the parametric nature allows for easy redesign and evaluation of not only the aircraft, but also the fuel system.

3.1.1. Total fuel burn

According to Rajaram *et al.* [6], an aircraft subsystem can affect four parameters: weight, zero-lift drag, shaft power off-take, and bleed air off-take. The way they eventually lead to fuel burn is presented in Fig. 3.1. Each line represents an analysis module, some of which can be evaluated using PHALANX. In fact, only lines 1-3 are to be developed in this thesis. Number 1 represents the weight of the fuel and the fuel system and their effect of the balance of the aircraft, number 2 represents the required shaft power off-take, and number 3 represents the conversion from instantaneous fuel flow to the fuel burn over a mission. The other lines can be evaluated using PHALANX.
A subsystem does not necessarily affect all parameters; internal systems such as the air conditioning packs will not affect zero-lift drag. Figure 3.1 must therefore be adapted to fit the subsystem one is interested in. It is clear that a fuel system will have significant influence on the weight and balance of the aircraft. In the DC-10-10 and the F-28 the fuel system amounts to 0.802% and 0.816% of the manufacturer's empty weight, which is the equivalent of 840kg and 108kg, respectively [37]. At takeoff, the fuel may amount for 40% of the aircraft takeoff weight. Hence there should be no debate about the fact that the fuel (system) has a large influence on the induced drag, both through the gross weight and consequences on the CG. Regarding shaft power off-take, Seresinhe and Lawson [25] found that the fuel system is responsible for roughly 8% of the aircraft electrical power consumption, which appears significant enough to warrant the modeling of the fuel system's power off-take.
Two other ways in which aircraft subsystems influence fuel burn are changes in zero-lift drag, and bleed air off-take. For fuel systems specifically, it depends on the design choices whether or not this is the case. Some aircraft employ external fuel tanks to increase their range, and it is not unthinkable that the wing planform or fuselage shape is altered to increase the fuel tank's capacity [38] [39]. Moreover, vented fuel systems for civil aircraft often have scoops near the tips of the wings to slightly pressure the tank ullage [5]. Such scoops indeed come with an aerodynamic penalty and are strictly speaking part of the fuel venting system. This thesis, however, does not deal with the venting system, assumes that the fuel tanks will not alter the aerodynamic shape of the aircraft and merely attempts to create a fuel system given any aircraft shape.
As is the case for zero-lift drag, it depends on the design choices whether or not a fuel system has any bleed air off-take. One will find that military aircraft pressurise their fuel tanks to increase the dive, climb, and altitude capabilities of the aircraft, as is reflected in the model used by [22]. Again, this thesis is focused on civil aircraft, which have no need for tank pressurisation.
Boggero [23] proposed a workflow where a feedback loop is present between the initial layout and the on-board systems sizing. For fuel systems, changes in the fuel flow may demand the redesign of the fuel pumps, hence a feedback loop between the fuel flow and subsystem may be required. Additionally, significant changes in the fuel burn may lead to different tank size requirements, creating the need for a feedback loop between the fuel burn and the fuel system.

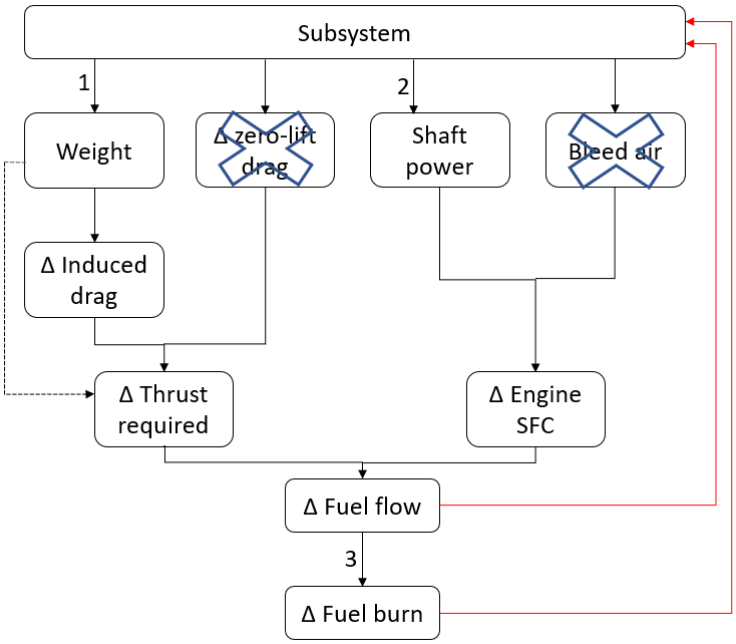

Figure 3.1: Impact of fuel system on fuel burn, adapted from [6]. Adaptations in red.

3.2. Information Exchange

Figure 3.2 shows how information is exchanged between the MMG, VSAERO, PHALANX, and the fuel system design and simulation modules. The figure is an adaptation from [40], where all contributions from this thesis are presented in red. All shaded boxes represent analysis modules, and any box without an arrow pointing towards it represents an input.

The analysis of a fuel systems starts with an instance of an aircraft in the MMG, generated from full-scale model geometry parameters. The MMG geometry model is built in the ParaPy environment, meaning that it is possible to extract the 'building blocks' of an aircraft (i.e. parts and attributes). The building blocks required for the fuel system design module include the wings, leading and trailing edge points of the wings, fuselage, floor, and engine. The other input for the fuel system design module is a set of fuel system design choices. The design choices are made in a .json-file and include locations for the tanks, routes for fuel lines, and options for equipment in each tank. These choices, and the workings of the fuel system design module are explained in more detail in paragraph 3.3.
The output of the design module can be divided into three categories. The tank geometry is a set of solids for the fuel tanks. By passing the solids, the ParaPy environment can be used in the simulation module to compute the volume and CG. The pump off-take database holds information on the power requirement for all pumps-destination combination in the system. This database is used in the simulation module to report on the power consumption of the system. Finally, the design module reports on the fuel system mass and CG, taking into account all pumps, valves, fuel lines, and sealant weight. The system mass is used to update the mass and inertia database fed to PHALANX by replacing the estimate for the fuel system mass and CG in [7] with the module's estimate.
The simulation module employs a time stepping scheme to simulate a cruise-only mission. The user provides an initial fuel distribution among the tanks in the form of a list. The simulation then loads the tank geometry and pump off-take database and starts iterating. For each iteration, the combined fuel mass across the tanks and the fuel CG is computed, and used to update the mass and inertia database for PHALANX. For the given flight condition (i.e. the cruise condition), PHALANX trims the aircraft by performing a steepest descent optimisation routine for a straight and level flight. In the trim results, the instantaneous fuel consumption is reported, which when multiplied by the time step is used by the simulation module to update the fuel mass and CG. All steps included in this routine are marked by dashed arrows in Fig. 3.2. When the combined fuel mass drops below 350kg, the simulation module

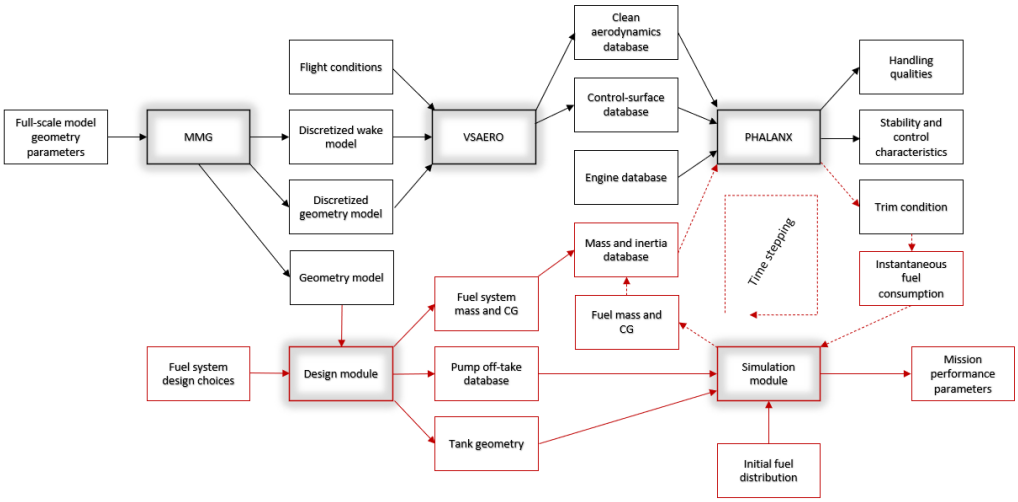

Figure 3.2: Information exchange between the MMG, VSAERO, PHALANX, and the fuel system module.

stops iterating and reports on the mission performance parameters. These include the total fuel consumption, power consumption, and a trace of the CG positions of the aircraft and fuel during the flight. The simulation module is discussed in more detail in section 3.4.

3.3. Design module

As is presented in Fig. 3.2, the design module has two groups of inputs, and three groups of outputs. In Fig. 3.3 the output of the MMG, i.e. the geometry model of the aircraft, is shown. Notice how the front wing is split into trunks, where each trunk has a different taper ratio. To deal with the taper ratios, the design module requires the leading and trailing edge points at the root and tip of the wing and the point where each trunk meets. For the creation of fuel lines and optional tanks in the fuselage, the user must also provide an instance of the fuselage, floor, front cabin wall, and aft pressure bulkhead. The keen eye will notice that the engine is missing from Fig. 3.3. Indeed, the design module only requires the point where the fuel line exits the fuselage or wing to the engine. Optionally, one can provide the locations of the fan and final turbine stage, such that the rotor burst zone can be determined. Later, the designer has the choice to truncate the fuel tanks such that do not coincide with the rotor burst zone, which is common practice for integral fuel tanks [5]. Also notice the coordinate system, the origin of which lies at the forward tip of the fuselage. The x-coordinate, increasing as one traverses to the aft part of the aircraft, is of particular interest as this thesis largely deals with longitudinal stability.

3.3.1. Creating the fuel system geometry

The user can now decide on the design of the fuel system through a .json-file. In a set of global settings, one chooses the system level properties such as the feed and transfer route(s), and the location of the crossfeed assembly. On the wing level, the user must define the locations of the front and rear spars, both of which are assumed to be uniform across the wing and expressed in a local chord parameter. Tanks can now be created by defining the parameters (ranging from 0 to 1) indicating the spanwise positions of the tank end points. It is possible to create multiple tanks, e.g. the parameters [[0, 0.3][0.5, 1]] will create two tanks spanning from the root to the tip, leaving a spanwise space between 0.3 and 0.5. The module will leave space for a vent box equal to some percentage of the fuel tank's volume specified by the user. The user must also specify whether the leading or trailing edge rail will be used as the transfer rail - the other rail will be used as the feed rail. These rails initially span the entire wing, and are used to connect the tanks.
At the tank level, the user can specify which interior equipment must be generated for each individual tank, where they must be placed, and if they must be present in the mirrored tank. The available interior equipment includes transfer outlets, refuelling stations, jettison pumps, (ETOPS compliant)

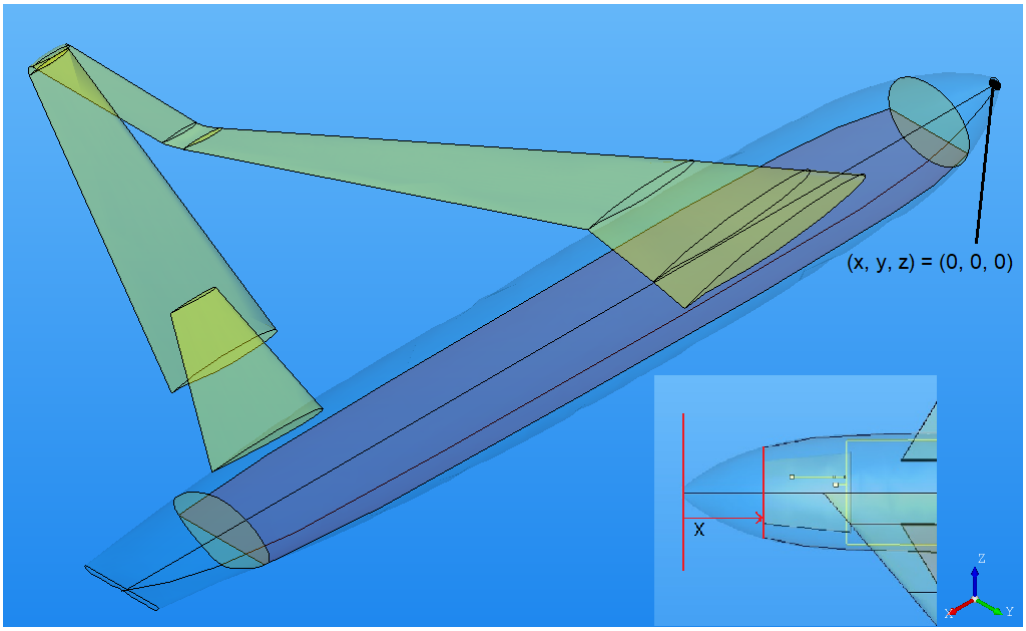

Figure 3.3: A box wing aircraft geometry model from the MMG, showing only the left hand side wings. Includes a top-down view from the nose of the aircraft, indicating the positive x-direction.

crossfeed assemblies, feed cells, and transfer pumps. The interior equipment is modeled using cylinders and boxes, and can be placed at the designer's discretion using parameters ranging form 0 to 1 indicating the spanwise and chordwise position in the tank.
In some cases the fuel lines will run underneath the fuselage floor, through the vertical tail(s), or the connecting elements between the upper and lower wings. These wings must be assigned a pass-through flag and wing level parameters must be provided such that the feed and transfer lines can be created. It is also possible to create a fuselage tank, for which the defining parameters are based on wall and floor clearances, instead of spanwise and local chord parameters.
The system is now almost complete; each wing has its tanks built, and each tank has its interior equipment built. To complete the system, all rails are connected by adding an element connecting the points at which the rails are closest. A dictionary is then created to store all the points where interior equipment is connected to the rails, and where the rails are connected to other rails. In order to avoid sections of fuel line that lead to nowhere, the rails (i.e. the fuel lines) are truncated at the most inboard and outboard connections point.
Figure 3.4 shows an annotated box wing aircraft fuel system geometry, its .json-file can be found in Appendix 7. Note that several mirrored components have been omitted from the figure for clarity's sake. Also note the option to cut off the tanks to avoid intersections with the rotor burst zone of the engine. In Fig. 3.4, the tanks are not cut off. Finally, note that in Fig. 3.4 there is only one scavenge pump for each feed cell aimed in the chordwise direction, which is present to keep the feed cell full at all times. The module is capable of placing an additional scavenge pump in the spanwise direction should there be any concerns that a single scavenge pump is not sufficient. By default, the module computes the dihedral of the underside of the trunk the feed cell is placed in, and the designer specifies the amount of dihedral for which it is no longer necessary to place the second scavenge pump. Alternatively, the designer can specifically request the feed tanks for which the second scavenge pump must be placed. The second scavenge pump also increases the fuel flow rate requirement for the feed pumps.

3.3.2. Mass estimation

From the geometry, the fuel system module is capable of estimating the mass and CG of the fuel system, and the fuel. ParaPy has a built-in functionality of finding the CG of any line segment, surface, or volume. Hence if one has access to a list of all components the fuel is comprised of, and their corresponding masses, then the CG of the system is found by simply:

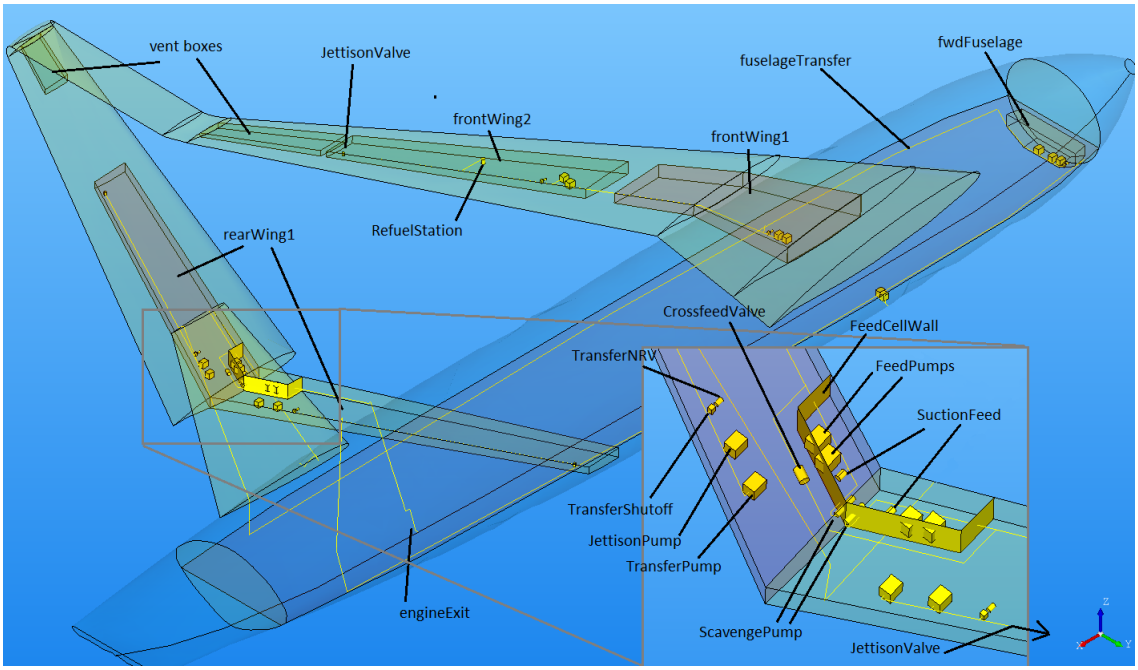

Figure 3.4: Fuel system geometry generated by the module.

Table 3.1: Number of valves and NRVs in interior elements

Interior	No. Valves	No. NRVs	Combined Weight
TransferOutlet	1	1	2.17kg
Jettison	0-1	1	0.11-2.17kg
MotorPump	0	1	0.11kg
Crossfeed	1-2	0	2.06-4.12kg
FeedCell	0	3	0.33kg
EngineExit	1	0	2.06kg

$$x_{cg} = \frac{\sum_{i=1}^{N} m_i \cdot x_i}{\sum_{i=1}^{N} m_i} \tag{3.1}$$

Where x_{cg} is the x-coordinate of the CG, N is the number of the components, m_i is the mass of each component, and x_i is the x-coordinate of the CG of each component.
At this point, a distinction is made between the fuel and the fuel system. The mass and CG of the fuel system itself does not change over the course of a mission - it is part of the static mass of the aircraft. The mass and CG of the fuel, however, change over the course of a mission. Relative fuel burn and transfer between fuel tanks causes the CG of the fuel to shift significantly, which in turn affects the aircraft's CG. The combination of a tank's shape and burning fuel may cause the CG of fuel inside a tank to shift, as caused by changes in attitude. For this thesis, it is assumed the attitude of the aircraft remains level for the entire mission. The CG trajectory of fuel inside a tank is approximated by cutting the fuel into 20 slices with equal spacing in the z-direction, recomputing the mass and CG of the fuel after a slice is taken away, and linearly interpolating between the results, see Fig. 3.5
The static mass of the fuel system is broken down into five categories: valves, non-return valves (NRVs), fuel lines, tank sealant, and pumps. The mass of any valve or NRV is assumed to be 2.06kg and 0.11kg, respectively, in accordance with the values reported in [41] and [42]. Table 3.1 presents the amount of valves and NRVs present in each interior element. The total mass of the valves and NRVs is found by multiplying the amount of valves and NRVs in the system by their respective masses.

The total weight of the fuel lines in the system is determined by multiplying the system line length with the linear mass density (kg/m) [43]. Fuel lines running through the pressurised fuselage receive

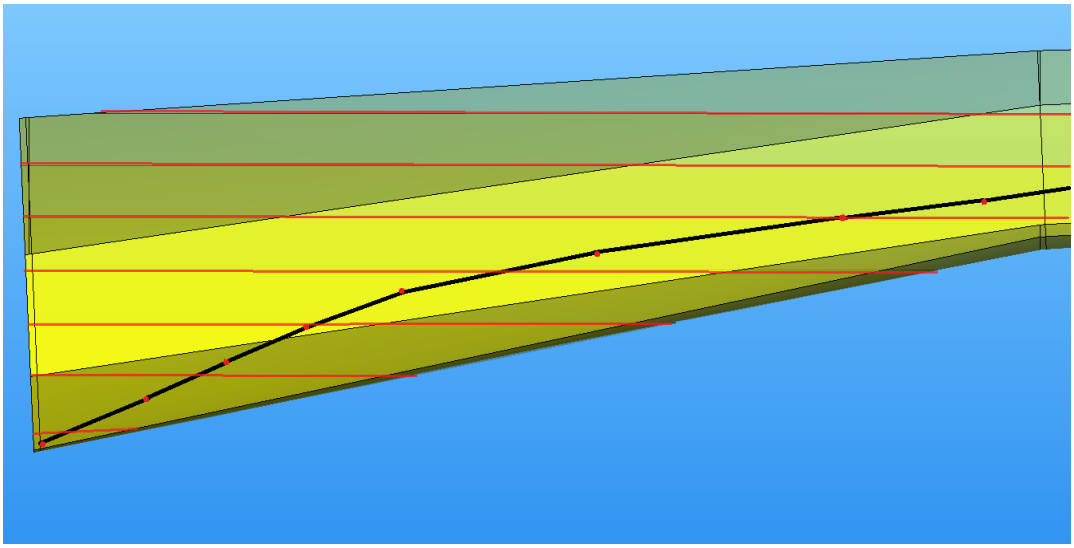

Figure 3.5: Graphical interpretation of fuel CG estimation, depicting the inboard portion of a fuel tank, cut into several slices (slices in red). The CG is computed for each slices (points depicted in red), and the CG excursion for different fuel loads is found by linearly interpolating between the CGs (line in black).

a linear mass density penalty, as they are often double-walled to avoid leakage [5]. To find the system line length, the module uses a 'highway' system, where the fuselage and the wings are equipped with transfer and feed highways spanning the complete part. The parts are then connected by creating a line segment at the point where the two lines are closest. All interior elements, i.e. the pumps, transfer outlets, etc., are connected to this highway system. Hence each highway can be truncated at the outermost connection points with interior elements, cutting away any segment that leads to nowhere. Summing the length of each remaining segment leads to the system line length.
The mass of the tank sealant is assumed to be dependant on the combined length of the edges of the tank. The rationale is that the plates that make up the surface of the tank do not need sealing, but their connecting edges do. Of course, this disregards any sealant that might be required for any bolts or rivets in the tank surface. Similarly to the fuel lines, the edge length is multiplied by its linear mass density, which was found by creating a reference Fokker 100 fuel system, finding the combined edge length, and setting the linear mass density such that the resulting sealant mass matches the mass reported in [8].
Pump sizing is performed with the use of a least-squares linear regression using the data of pre-existing fuel pumps. More specifically, the power requirement was extracted from pump data sheets and plotted versus the weight of the pump (Fig. 3.6), resulting in a linear trendline which was implement in the module. The power requirement of the pump is determined using the method presented in [43]:

$$P = \frac{\dot{V} \cdot \Delta p_{req}}{R} \tag{3.2}$$

Where P is the engine feed power, $\dot{V}$ is the fuel flow rate, Δp_{req} is the required pressure, and R is the engine feed flow reduction factor. The latter accounts for the effects of cavitation in the fuel lines and boost pump, which limits the flow rate:

$$R = \frac{\Delta p_t + p_{atm} - \Delta p_{f_{low}} + p_h - p_{R=0}}{p_{R=1} - P_{r=0}} \frac{1}{c_p} \tag{3.3}$$

Where p_{atm} is the atmospheric pressure, $\Delta p_{f_{low}}$ are the friction losses of the pump inlet, $p_{R=1}$ is the pressure at which cavitation starts to develop (which corresponds to $70000Pa$), $p_{R=0}$ is the pressure at which cavitation is fully developed (corresponding to $17000Pa$), and c_p is the pump's tendency for cavitation. The required pressure Δp_{req} is given by:

$$\Delta p_{req} = p_{del} - p_t + \Delta p_{sys} \tag{3.4}$$

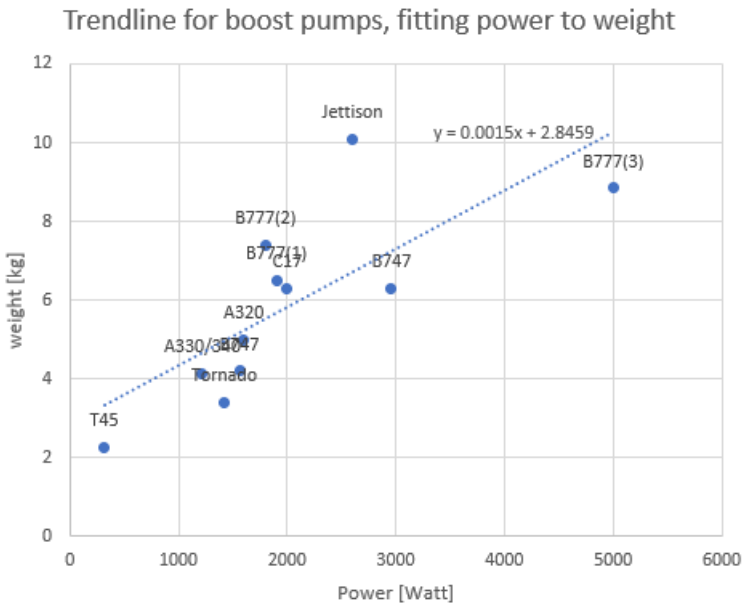

Figure 3.6: Trendline for boost pumps, fitting the power of the pump to the weight of the pump.

Where p_{del} is the delivery pressure, p_t is the pressure in the tank wherein the pump is placed, and Δp_{sys} are the pressures losses encountered in the system. The delivery pressure p_{del} is dependant on the application of the pump, e.g. for feed pumps it equals the feed pressure required by the engine manufacturer, while for jettison pumps it equals the atmospheric pressure. Finally, the system pressure losses are given by:

$$\Delta p_{sys} = (\Sigma K + \frac{4fl}{D})\frac{1}{2}\rho V^2 + \rho g(h_2 - h_1) = \Delta P_f + \Delta P_h \tag{3.5}$$

Where ΣK is the sum of the friction factors of the corners and valves along the route, f is the pipe friction factor, l is the pipe's length, assumed constant across the system, D is the pipe's diameter, ρ is the fuel density, V is the flow velocity, g is the gravity constant, h_1 is the height of the fuel pump, and h_2 is the height of the fuel line outlet.

Using this system of equations, any pump in the system can be sized, no matter the application and operating condition. To size a boost or transfer pump, two cases are considered: a takeoff case and a cruise case. For takeoff, the atmospheric pressure is set to sea level, and the velocity is set to zero, i.e. the tanks are not pressurised as a result of the air scoops. For cruise, the atmospheric pressure is set to 11.000m in accordance with the ISA model [44], and the tanks are pressurised to 1.3 times the atmospheric pressure [5]. Jettison pumps, on the other hand, are sized to operate at FL050, with a tank pressure ratio of 1.1 with respect to the atmospheric pressure [5].
It is true that Equations 3.2-3.5 are rather basic, yet plugging the correct values has proven to be a real challenge. Langton *et al.* [5] note that values for K are greatly dependent on the designer's experience and may range from 0.3 to 6. Even more so, the feed pump's flow rate also depends on the amount of jet (e.g. scavenge) pumps in the system. Additionally, the pressure requirement at the engine inlet differs from engine to engine and may range from 20psi to 35psi. Table 3.2 summarises the constants used in the pump sizing method for each application, along with corresponding rationale or source.

3.3.3. Shaft power off-take

The shaft power off-take of the system is determined by the pumps. Equation 3.2 has already shown how the power off-take is determined for the pumps. Now, the pump power off-take must be converted to shaft power off-take, which should lead to fuel burn. In [46] the following equation is presented:

Table 3.2: Values for variables used during pump sizing.

Variable	Value	Unit	Rationale / Reference
Fuel flow at cruise	0.66	kg/s	PHALANX engine map
Atmospheric pressure at cruise	22700	Pa	ISA FL360 [44]
Tank pressure ratio at cruise	1.3	-	[5]
Fuel flow at takeoff	1.24	kg/s	PHALANX engine map
Atmospheric pressure at takeoff	101325	Pa	ISA FL0 [44]
Tank pressure ratio at takeoff	1	-	No pressurisation since aircraft is at standstill
Atmospheric pressure at jettison	84300	Pa	ISA FL050 [44]
Tank pressure ratio at jettison	1.1	-	[5]
Fuel transfer rate ratio	1.5	-	Assumed 1.5x the fuel consumption, such that fuel can simultaneously be transferred to feed tank (1x) and to another tank (0.5x)
Fuel jettison rate ratio	5	-	Ultimately dependent on aircraft climb performance
Fuel density	804	kg/m3	
Engine feed pressure	20	psi	Lowest engine feed pressure found for a set of modern turbofan engines
Cavitation propensity	0.6	-	[43]
Friction factor valves	1.5	-	Based on one shutoff valve and one non-return valve [5]
Friction factor line bend	40D	-	40x the line diameter [45]
Cavitation development start	70000	Pa	[43]
Cavitation fully developed	17000	Pa	[43]
Pipe diameter	0.05	m	Based on recommended velocity of 10ft/s and initial fuel flow estimate [5]
Line density	0.3	kg/m	[43]

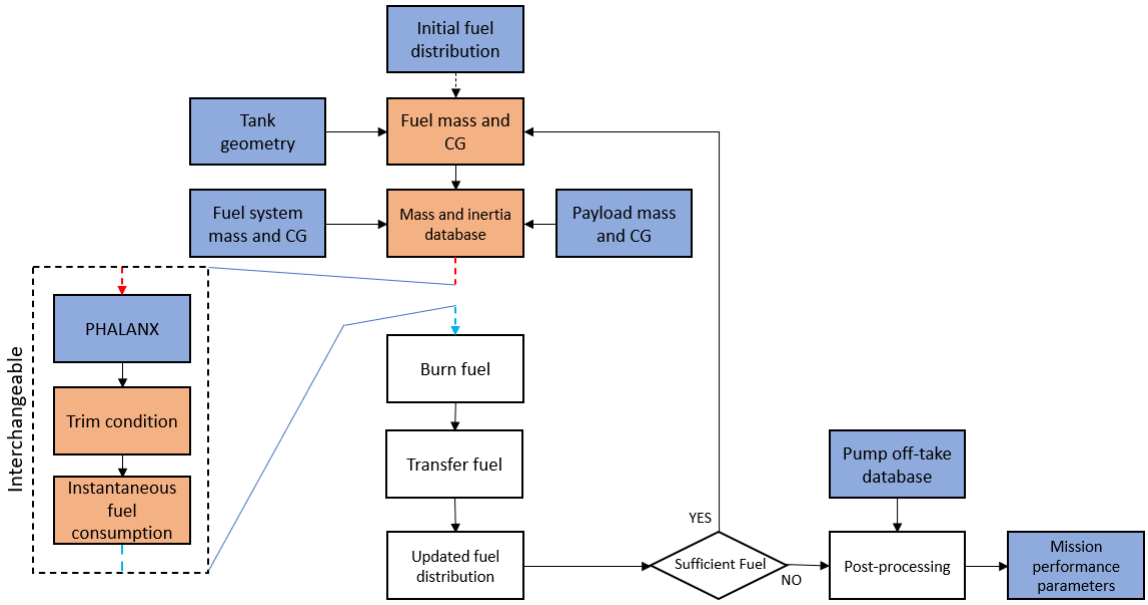

Figure 3.7: An overview of the simulation module.

$$\dot{m}_{F,P} = k_p \cdot SFC \cdot P \tag{3.6}$$

where $\dot{m}_{F,P}$ is the fuel consumption due to the power off-take, $k_p \approx 0.00225 N/W$ is the shaft power factor in Newton per Watt, SFC is the specific fuel consumption, and P is the pump power. Since the right-hand side variables are known for the aircraft of interest, Equation 3.6 can be used as-is.

3.4. Simulation module

The objective for the simulation module is to assess the performance of a fuel system. The mission performance parameters include the total fuel burn, and the operational flexibility. Figure 3.7 shows the workflow of the simulation module in more detail. Recall that the simulation module employs a time stepping scheme, so some blocks may contain different information at each iteration. Blocks that are also included in Fig. 3.2 and that contain the same information for each iteration are in blue. Blocks that are also included in Fig. 3.2 and that contain different information for each iteration are in orange.

3.4.1. Simulation Overview

In order to start a simulation, the user must first instantiate a fuel system in the design module. This instance will provide the simulation module with information on the tank geometry, which allows the estimation of the CG of the fuel in accordance with Fig. 3.5. The instance also provides the pump off-take database in the form of a look-up table with data on the power consumption of the transfer, feed, and jettison pumps (although jettison pumps are not used in the simulation) for all pump-destination combination. Finally, the design module instance provides a fuel system mass and CG estimation used to update the mass and inertia database. The user then chooses an initial fuel distribution and payload mass and CG. All information required to run the simulation is now in place.

From the tank geometry data and the initial fuel distribution, the new fuel mass and CG are computed. When looking at Fig. 3.7, one will notice that with the arrow from the initial fuel distribution to the fuel mass and CG is dashed. This is to indicate that the initial fuel distribution is only used in the first time step and is later overridden by the update fuel distribution.

Next, the mass and inertia database is updated with the fuel mass and CG. For the box wing aircraft, this database is comprised of data presented in [7]. The data is comprised of a weight breakdown of the aircraft, and the inertia for an aircraft at maximum takeoff weight (MTOW) with 25% of the mission fuel in the rear wing, and 75% of the fuel in the front wing. The version of PHALANX used in

this thesis approximates the inertia contribution of the fuel by a single point mass at the combined fuel CG. It is possible to use the tank geometry from the design module to provide an improved contribution of the fuel's contribution to the aircraft inertia. However, it has proven to be too time consuming to implement such a change to PHALANX.
Regardless, PHALANX is used to evaluate the trim condition for a straight and level flight at 11.000m altitude, and a velocity of 233.11m/s. Keep in mind that the aircraft can be trimmed even at dynamically unstable points, and that the inertia database is not required to trim the aircraft. It is assumed changes in the design cause sufficiently small changes in the inertia that it is warranted to leave the inertia of the aircraft unchanged, and only update the point mass contribution of the fuel. The stability of the aircraft is also not re-evaluated. The reader is referred to section 3.5 to understand how stability is dealt with.
The instantaneous fuel consumption is now extracted from the trim condition. By multiplying the instantaneous fuel consumption with the user defined time step, the fuel consumption for the time step is computed. The default time step is set to 5 seconds. The following blocks indicate that fuel is burned and transferred, after which the fuel distribution is updated. The available strategies with which fuel is burned and transferred are discussed in section 3.4.2.
The following decision block checks if there is sufficient fuel left to continue the mission. By default, the module will stop when there is less than 350kg fuel left in the system. If there is sufficient fuel, the updated fuel distribution will be used to update the fuel mass and CG, leading to a renewed mass and inertial database, and PHALANX is hailed again to determine the fuel flow. When there is insufficient fuel to continue, the module will gather the data from the previous time-steps, allowing the user to see the trajectories of the fuel and aircraft CG, and the total power consumed by the system as a result from fuel burn and transfer.

3.4.2. Fuel burn strategies

In Fig. 3.7 it is shown that when the instantaneous fuel consumption is known, fuel is burned, transferred, and the fuel distribution is updated. While this is essentially correct, it is a simplification of the actual fuel burn strategy. In fact, the model has two available fuel burn strategies: a pre-set burn sequence, and an active CG control scheme. The schemes are powerful tools for finding the operational flexibility, and the fuel burn for a mission, respectively.

Pre-set burn sequence

The pre-set burn sequence schematic is presented in Fig. 3.8. Here, the simulation distinguishes between feed tanks and auxiliary tanks, where feed tanks are equipped with a feed cell and are capable of directly feeding the engine. Auxiliary tanks are only equipped with transfer pumps and are strictly used to fill the feed tanks. One tank in the system can be assigned to be active. When the active tank is a feed tank, the engine is fed from that feed tank, and no transfer takes place between the other tanks. When the active tank is an auxiliary tank, the amount of fuel burned for that iteration is transferred from the active auxiliary tank to the feed tank. The same amount is also burned from the feed tank. The result is that the feed tank will hold the same amount of fuel after the iteration.
The user can define the burn sequence by defining a sequence of active tanks. Each entry in the sequence must be accompanied by a threshold value. Each iteration, the algorithm checks if the amount of fuel in the active tank is smaller than the current threshold value. If so, the algorithm updates the active tank to the next one in the sequence, and accordingly updates the threshold value. Once the final threshold value is reached, the simulation stops and enters post-processing.

The pre-set burn sequence is not aimed at optimising the fuel burn strategy in any way. Instead, serves its purpose as an analysis tool. With prior knowledge from the design module on the locations of the tanks and the corresponding CG traces of the fuel, one can define sequences that define the operational limits of the fuel system. For example, suppose that one is interested in the most forward CG during a mission for a box wing aircraft with one tank in the rear wing, and one tank in the front wing, and that both tanks are full at the start of the mission. The most forward CG can now be found by defining a sequence wherein the tank in the rear wing first burns all its fuel. When there is no more fuel left in the rear wing, the fuel in the front wing is burned. The resulting CG traces will be indicative

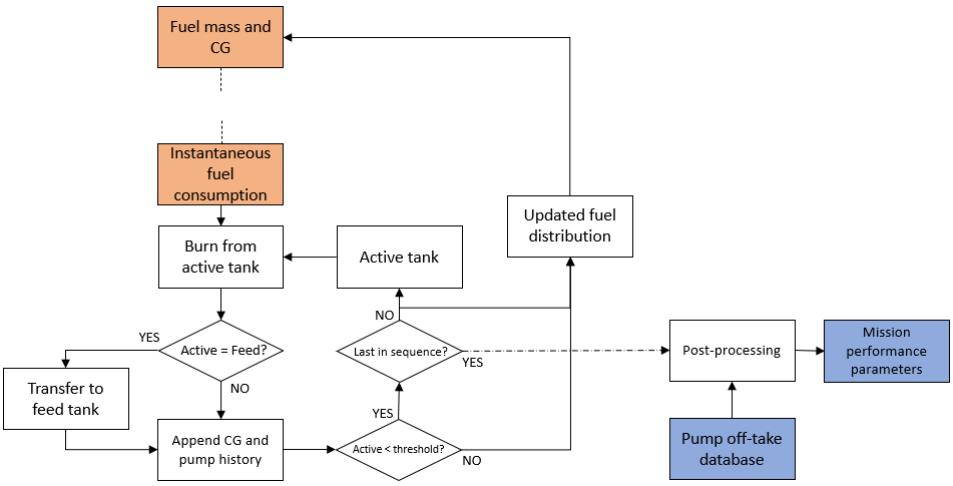

Figure 3.8: Pre-set burn sequence schematic.

of the fuel system's potential to move the CG forward.
Suppose that one is interested in finding a fuel system's potential to move the CG forward and aft, i.e. the operational flexibility that the fuel system allows for. By defining two burn sequences, one with the most forward CG and one with the most aft CG, the range over which the CG can be moved can be defined. In this case, the fuel consumption does not have to be an accurate guess, as long as it is burned until there is no fuel left.
Notice how Fig. 3.7 denotes the combination of blocks for PHALANX, the trim condition and the instantaneous fuel consumption as interchangeable. Indeed, these blocks can be replaced by any analysis module that results in an instantaneous fuel consumption. When one is interested in the CG range, the three blocks can be replaced by a unit fuel flow of 1kg/s, and the CG analysis would still hold. Additionally, using unit fuel flow ensures that both analyses for the most forward and aft CG have an equal number of iterations. Hence the following equation can be used to find the mean CG range:

$$\widehat{CG} = \frac{\sum_{i=1}^{N}(MAC_{max_i} - MAC_{min_i})}{N} \tag{3.7}$$

Where $\widehat{CG}$ is the mean CG range, N is the number of iterations, MAC_{max_i} is the aft MAC limit at step i, and MAC_{min_i} is the forward MAC limit at step i.

Active CG control

Where the pre-set burn sequence is useful for determining the mean CG range, the active CG control mode is useful for determining the fuel burn for a cruise-only mission. Figure 3.9 shows the flowchart for the active CG control scheme. Again, the interchangeable analysis module from Fig. 3.7 is not shown. It will become clear, however, that for this scheme it is best to have an accurate estimate of the fuel flow.
In this scheme, the tank sensitivities are a deciding factor in the resulting burn sequence. The sensitivity of a tank indicates what happens to the fuel CG when the amount of fuel in the tank decreases, either because fuel is fed to the engine, or because fuel is transferred to another tank. The sensitivity is either positive, negative, or zero. Positive sensitivity indicates that the fuel CG moves aft when the amount of fuel decreases in the tank, whereas negative sensitivity indicates that the fuel CG moves forward when the amount of fuel decreases in the tank. Zero sensitivity indicates that there is no change in the fuel CG when the amount of fuel in the tank decreases.
The active CG control scheme aims to minimise the amount of fuel that is moved around, under the assumption that this will result in the least amount of pump power required. The rationale is that the tank sensitivities can be compared against each other to determine which tank is most effective at performing a certain task. For example, if one finds themselves in a situation where the CG must be moved forward, fuel can be transferred from the tank with maximum sensitivity to the tank with the

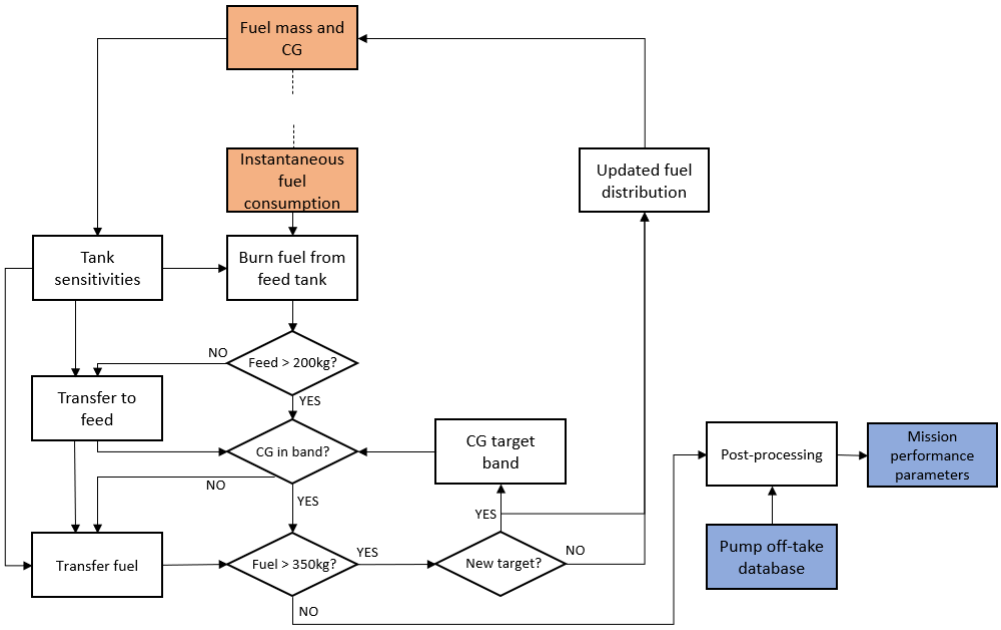

Figure 3.9: Active CG control schematic.

minimum sensitivity. This ensures that the least amount of fuel must be transferred by the system, minimising the activity of the transfer pumps.
Using this rationale results in the following decisions made by the system as portrayed in Fig. 3.9. Starting from the instantaneous fuel consumption, the system will burn fuel from the feed tank that has the minimum absolute sensitivity. This ensures that fuel burn causes the smallest shift in CG possible. Next, if that feed tank now holds less than 200kg of fuel, fuel is transferred to that feed tank from the auxiliary tank with the minimum absolute sensitivity. Afterwards, if the CG is no longer within the target band, fuel is transferred between the tanks with the minimum/maximum sensitivity. Depending on whether the CG is in front or aft of the target band, the tank with the maximum sensitivity will be the recipient or donor.
The CG target band is defined by the user by specifying a target x-coordinate for the CG, and the maximum allowable error. The x-coordinate is defined as running along the fuselage, pointing from the nose to the tail, where $x = 0$ coincides with the nose of the aircraft. Like with the pre-set sequence burn, the user can provide a sequence of CG target bands which are activated at user-specified fuel masses. The reader is referred to section 3.4.4 for the rationale deciding on the CG targets used in this thesis.
The transfer gallery is assumed to have a maximum fuel flow rate of 1.5 times the initial cruise fuel flow rate. This is to ensure that when the feed tank runs empty, the transfer system will be capable of supplying a surplus of fuel to the feed tank, where the surplus can be used for active CG control purposes. Each iteration, the algorithm keeps track of the amount of fuel that is transferred using the transfer gallery, ensuring that the transfer gallery maximum fuel flow rate is not exceeded.

3.4.3. Surrogate model

Recall that this thesis is aimed at the preliminary design and analysis of fuel systems. The preliminary nature in particular means that the module will likely be used to investigate a large number of designs. It is therefore important to realise that the analysis of a fuel system should be computationally cheap, and that the simulation module should take a limited time to complete. Admittedly, the choice for using PHALANX was mostly driven by the ease of access to such a powerful analysis tool. While it is quite clear that PHALANX has its merits regarding the accuracy with which fuel consumption is estimated, there are also drawbacks to its use. More specifically, using PHALANX in the simulation loop is computationally demanding, and the tool requires an aerodynamic database and engine model corresponding to the aircraft of interest.

For the purposes of this thesis, a surrogate model has been developed which can be used in the interchangeable block from Fig. 3.7. Indeed, the creation of the surrogate model is (very) time-consuming, and it is only valid for the box wing aircraft presented in [7]. However, the surrogate model significantly reduces the computational cost of the simulation module, and efforts have been made to ensure that as long as the aircraft of interest does not significantly deviate from the reference design presented in [7], any fuel system can be evaluated. Finally, the possibility to change the payload of the aircraft has been retained.

Response surface

At its very core, the surrogate model is an 4D-interpolant created from a set of control points extracted from PHALANX. The 4 dimensions are 1) the x-coordinate of the fuel CG, 2) the fuel mass, 3) the payload mass, and 4) the fuel flow. During a mission, the payload is constant, whereas the other three dimension vary. Since the payload mass is a fixed value, it is possible to create a response surface for any mission. Such a response surface is shown in Fig. 3.10, where the x-axis represents the x-coordinate of the fuel CG, the y-axis represents the fuel mass, and the z-axis (represented as a heat map) represents the fuel flow. The (irregular) grid intersection points represent the control points of the interpolant. The y-coordinate of the fuel has not been included as an input, because the fuel is assumed to be symmetrical. The z-coordinate of the fuel has not been included as an input because an initial investigation of the fuel flow revealed that its influence is insignificant compared to the other parameters. The influence of the z-coordinate is negligible, because the contribution of the interaction between the thrust vector and the aircraft CG to the moment equation is small. Even more so, despite the height difference between the tanks, the fuel system is ill-equipped to control the z-coordinate.
The most prominent feature in Fig. 3.10 is perhaps the lack of data in the top left and right corners. This lack of data is related to the stability of the aircraft. Recall that the instantaneous fuel flow is extracted from the PHALANX trim condition, and that this would require that the aircraft can be trimmed. Now consider that the y-axis represents the fuel mass. Indeed, when the fuel mass increases, its effect on the CG of the aircraft also increases. With the reference aircraft approximately 40m in length, it should be no surprise that when the fuel mass is increased, the range of fuel CG over which the aircraft can still be trimmed starts to converge towards the CG of the aircraft at around 21.5m.
This rationale can also works vice-versa for low fuel masses. Fig. 3.10 shows that when the fuel mass decreases, the amount of control points along the x-axis (the x-coordinate of the fuel CG) increases. Even more so, it seems that the trimmable fuel CG range extends beyond the physical limits of the aircraft. Indeed, if the aircraft can be trimmed when there is no fuel on board, then surely the aircraft can still be trimmed if 10kg of fuel is put at x=100m. Although this is not physically possible since x=100m is not within the confines of the aircraft, mathematically the aircraft can still be trimmed.

Surrogate fuel mass and CG

If it is not physically possible to store fuel outside the confines of the aircraft, why would one mathematically do so? The answer lies in the disparity between the aircraft used during the sampling of the response surface, and the aircraft generated by the design module. Recall that it is a requirement of the surrogate model to be able to assess different designs. The response surface is sampled using the reference aircraft. However, in case one wishes to assess a different design, one has to generate the design using the design module and load it into the simulation module. The simulation will then use this newly designed fuel system to update the mass and inertia database, but subsequently use the surrogate model, which was generated using the reference design. From this point onward, the aircraft used by the simulation module is referred to as the simulated aircraft, while the aircraft used to generate the response surface is referred to as the reference aircraft.
From Fig. 3.2 it is clear that PHALANX needs a clean aerodynamic database, control-surface database, engine database, and mass and inertia database to come to a trim condition. Earlier in this thesis, it is assumed that the fuel system has no effect on the aerodynamics of the aircraft. Since the fuel system does not affect the engine database, the mass and inertia database is the only database that is affected by changes in the fuel system design. This creates an opportunity to 'trick' the response surface into finding the correct fuel flow for the simulated aircraft.
During each iteration in the simulation module, the mass and CG of the aircraft, and the mass and

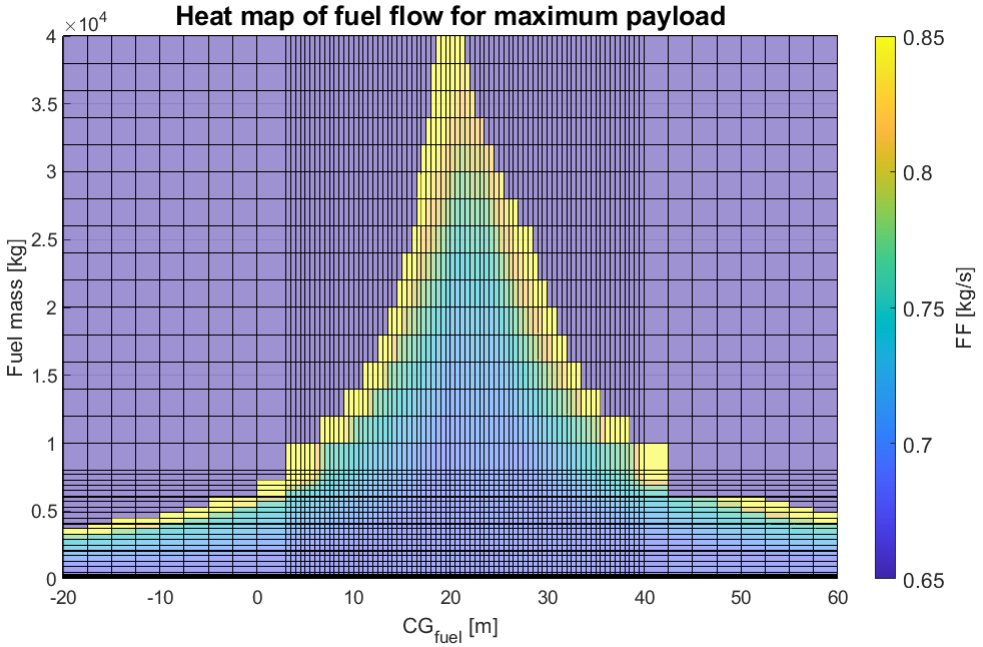

Figure 3.10: Response surface represented as a heat map, showing the fuel flow for different fuel masses and fuel CG combinations.

CG of the fuel are updated in PHALANX in order to find the new instantaneous fuel consumption. If the mass and CG of the simulated and reference aircraft are the same, then their instantaneous fuel consumption will also be the same same. The contributions to the mass and CG of the aircraft can be broken down into three categories: 1) the empty operating weight (EOW), 2) the payload, and 3) the fuel.
For the simulated aircraft, all three contributions are fixed; the EOW is generated from the design module, the payload was determined by the user at the start of the simulation, and the fuel is simulated by the module. For the reference aircraft, the EOW is fixed to reflect the aerodynamic and engine databases in PHALANX, and the payload and fuel are free to be chosen. The following equations can be used to ensure that the simulated and reference aircraft have the same mass and CG:

$$m_{eow_{sur}} + m_{pld} + m_{f_{sur}} = m_{eow} + m_{pld} + m_f = m_{ac} \tag{3.8}$$

$$\frac{x_{eow_{sur}} \cdot m_{eow_{sur}} + x_{pld} \cdot m_{pld} + x_{f_{sur}} \cdot m_{f_{sur}}}{m_{ac}} = \frac{x_{eow} \cdot m_{eow} + x_{pld} \cdot m_{pld} + x_f \cdot m_f}{m_{ac}} \tag{3.9}$$

Where x is the x-coordinate of a CG position, m is a mass, the sur sub-subscript denotes the surrogate model, the eow subscript denotes the empty operating mass, the pld subscript denotes the payload, the f subscript denotes the fuel, and the ac subscript denotes the aircraft. Variables without a sub-subscript represent simulated values. Notice the left hand sides of the equations (representing the surrogate aircraft) do not use a surrogate payload mass and CG, i.e. the payload mass and CG are the same for both aircraft. This is done to create a system with an equal amount of equations and unknowns. Consequentially, the disparity between the simulated and reference aircraft is entirely compensated for in the surrogate fuel mass and CG.
Consider an example where the simulated aircraft is 10kg lighter than the reference aircraft, and the CG of the simulated aircraft is slightly in front of the CG of the reference aircraft. According to equations 3.8 and 3.9, the surrogate fuel mass will always be 10k less than the simulated fuel mass. The surrogate fuel CG will be forward of the simulated fuel CG, and the difference between the two will be a function of the simulated fuel mass. This difference may become quite substantial, however, and is the reason that the response surface from Fig. 3.10 is extended beyond the physical limits of the

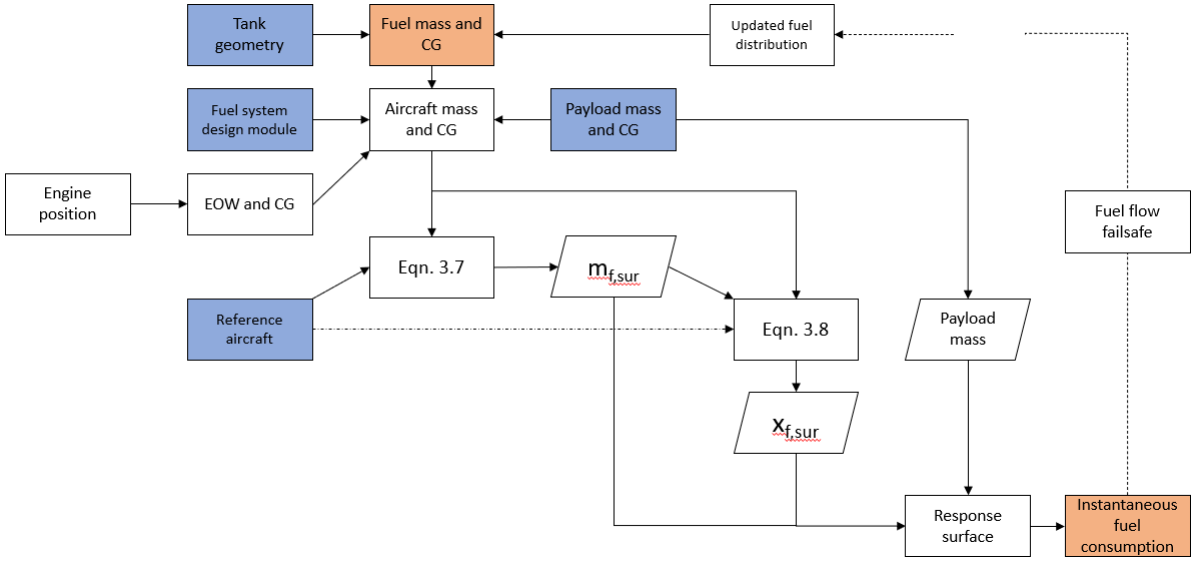

Figure 3.11: Surrogate model schematic.

aircraft.

Using the surrogate model

The interface of the surrogate model with the simulation module is presented in Fig. 3.11. Starting from the simulated fuel mass and CG, the simulated aircraft mass and CG are calculated using the fuel system design module weight breakdown, and the payload mass and CG. There is also the option to change the engine position in the x-direction and its effects on the aircraft CG are taken into account. Next, Equation 3.8 is used to ensure the masses of the simulated and surrogate aircraft are the same, resulting in the surrogate fuel mass $m_{f_{sur}}$. Using the surrogate fuel mass, Equation 3.9 is used to ensure the CG of the simulated and surrogate aircraft are the same, resulting in the surrogate fuel CG $x_{f_{sur}}$. With the payload mass and surrogate mass and CG known, the response surface can be used to find the instantaneous fuel consumption.

Notice that the instantaneous fuel consumption must pass the fuel flow failsafe block before the simulation module updates the fuel distribution. This failsafe block is not needed when the surrogate model is not used, because PHALANX will fail to converge to a trim condition, halting the simulation. For the surrogate model, when PHALANX fails to converge, the corresponding control point value is set to zero. This is done to allow the creation of the response surface, since full matrix of size $N \times M \times K \times I$ must be provided. Suppose that the simulation module starts at a point where the surrounding control points have not converged, and the interpolant returns zero fuel flow. Now, the simulation module is stuck in an infinite loop where no fuel is burned, hence the need for the fuel flow failsafe. The failsafe stops the simulation whenever the response surface returns a fuel flow that is larger or smaller than the largest or smallest non-zero fuel flow at any control point in the matrix, respectively. This inherently means that when using the surrogate model, the simulation will stop whenever the aircraft can no longer be trimmed.
This does not, however, mean that the simulation stopped when the aircraft is unstable. In fact, Fig. 3.12 contains many unstable control points. To illustrate, Fig. 3.12 shows the low-speed and high-speed stability limits from [7] are plotted on the surrogate model response surface. The low-speed stability limit represent the approach flight conditions, and the high-speed limit represents the cruise flight conditions. To plot a stability limit, Equation 3.9 was used, where the right hand side of the equation was simply replaced by the stability limit. This results in the two curved plotted in Fig. 3.12 that show all the combinations of fuel mass and CG that result in an aircraft CG that corresponds with the stability limit. Note that for the box wing aircraft, the aircraft CG should be in front of the stability limit for the aircraft to be stable: $x_{ac} < x_{stablimit}$.

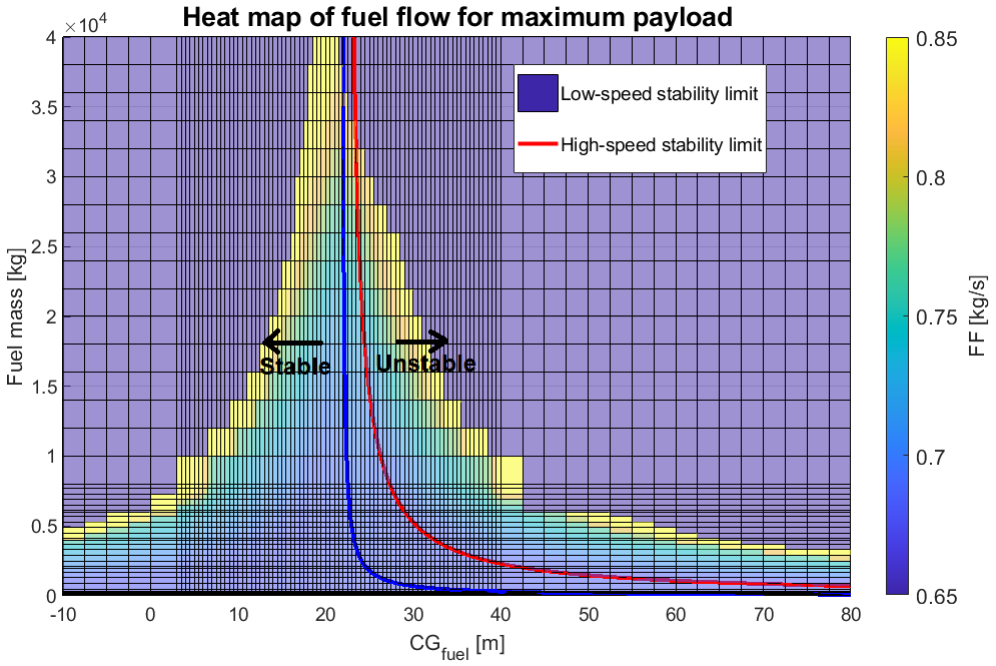

Figure 3.12: Response surface represented as a heat map, showing the fuel flow for different fuel masses and fuel CG combinations, including low- and high-speed stability limits.

Any control point to the right of the stability limits presented in Fig. 3.12 is unstable, and the user must check during post-processing if this limit is reached. It is clear from the figure that the low-speed stability limit is more forward than the high-speed stability limit. Unfortunately, there is no data regarding the controllability limit of the aircraft. In [7] it is reported that the reference aircraft is controllable for three specific flight conditions, but no actual limit is mentioned. Fortunately, results will later indicate that the stability limit is often the deciding limit.

Building the surrogate model

Figures 3.13 and 3.14 are two 3D plots of the surrogate model response surface. Again, the x-axis corresponds to the fuel CG x-coordinate, the y-axis represents the fuel mass, and the z-axis represents the fuel flow. This time, however, the figure is in 3D. The payload is kept constant for both plots, and the surface colours represent the z-axis, i.e. the fuel flow. Notice how for Fig. 3.14 the x-axis stretches far beyond the physical confines of the aircraft. The point of both figures is to show how the domain is surrounded by ridges. When the CG of the fuel is moved far to the left or the right, both figures show that one will encounter a ridge where the fuel flow substantially increases, before it drops to zero, indicating an aircraft that cannot be trimmed.

The ridges are partly the result of the discontinuity at the edge of the trimmable domain. While the fuel flow does tend to increase when the edge of the trimmable domain is reached (due to excessive control surface deflections, angles of attack, and thrust settings), interpolations methods are notoriously bad at dealing with discontinuities. It is not uncommon that interpolation of a function function discontinuity results in large undulations around the discontinuity [47]. Among the available MATLAB interpolation methods, the modified Akima cubic Hermite interpolation method was observed to be best capable of interpolating the curved domain while suppressing edge undulations.

For $10 < x < 30$ one can see that there are a lot of fuel-CG combinations that lead to a fuel flow, and that the ridges are essentially a non-factor. However, at low fuel masses and CGs outside the physical confines of the aircraft, the ridges still influence the result. In an attempt to suppress this effect, the control points grid has been refined at low fuel masses, and extended to span from $-1000 < x < 1000$. Since calculating the fuel flow at the control points is computationally expensive, the was separated into four smaller, overlapping grids, such that the amount of control points in the untrimmable region was reduces. The grid step sizes and limits are presented in Table 3.3. The grids are combined in a

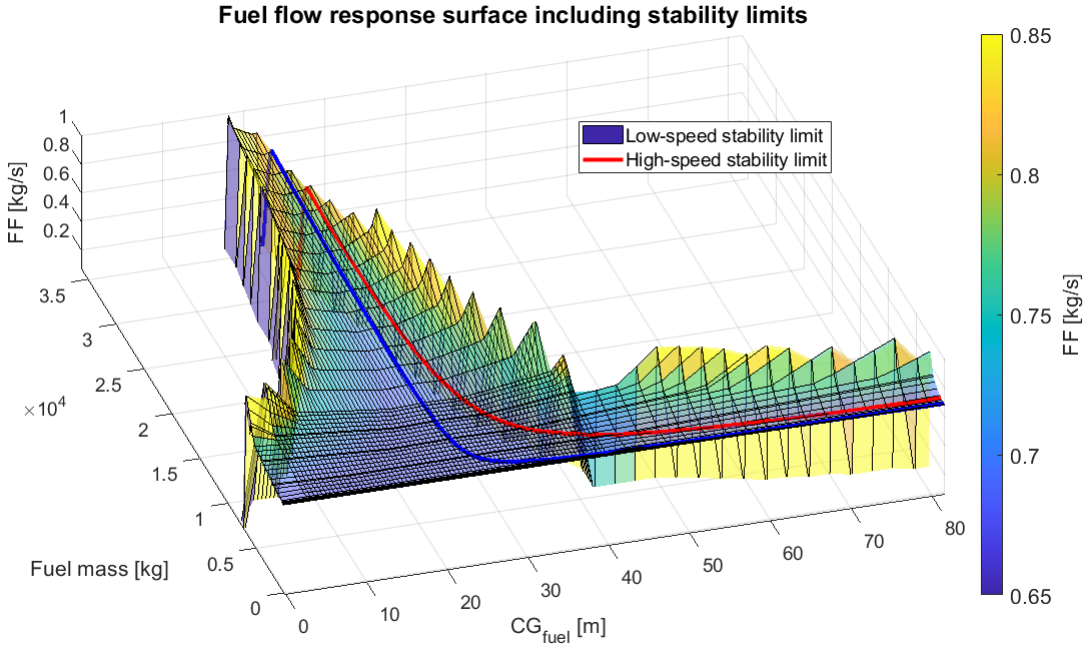

Figure 3.13: 3D fuel flow response surface, showing the fuel flow for different fuel masses and fuel CG combinations, including low- and high-speed stability limits, focusing on the physically feasible portion.

Table 3.3: All grid characteristics used to create the control point grid for the surrogate model.

Grid	CG limits	CG step size	Fuel mass limits	Fuel mass step size
1	3 < x < 40	0.5	0 < m < 40000	2000
2	-1000 < x < 10000	100	100 < m < 7900	100
3	-1000 < x < 1000	100	0 < m < 350	50
4	-80 < x < -2.5	2.5	500 < m < 5700	400
5	42.5 < x < 90	2.5	500 < m < 5700	400

larger matrix, from which the interpolant is created using the MATLAB griddedInterpolant function.

3.4.4. Optimal CG

The surrogate model response surface has the added benefit of being able to inspect what will happen to the fuel flow if the CG is changed. Figure 3.15 zooms in on the mid part of the response surface where the edge undulations are no issue. Again, the figure is a 3D representation, where the z-axis is limited to a small region in order to make changes in the fuel flow more visible. By also limiting the y-axis to 6000kg < fuel mass < 20000kg, two plane cuts are created which are highlighted in the Figure. The plane cuts reveal two valleys separated by a minor ridge, where the left valley is more fuel efficient than the right valley. The valleys also appear to converge when the fuel mass increases. Coincidentally, the valleys correspond to a certain CG of the aircraft. Two CG traces have been added to the figure corresponding to the aircraft CG of 21.54m and 21.56m. Both are close to the left valley, and thus it makes sense to use x=21.55m as the target CG, with a maximum allowable error of 0.01m. This target CG will be used for the remainder of this work. Indeed, this the optimal CG also lies within the flight envelope of the aircraft. Also note that the lower bound of 21.54m appears slightly less efficient than the upper bound.

3.5. Design of experiments

Recall the lead research question of this thesis that if, given the box wing aircraft, the opportunity of splitting the fuel over two large tanks in front and behind the aircraft CG can be exploited to achieve

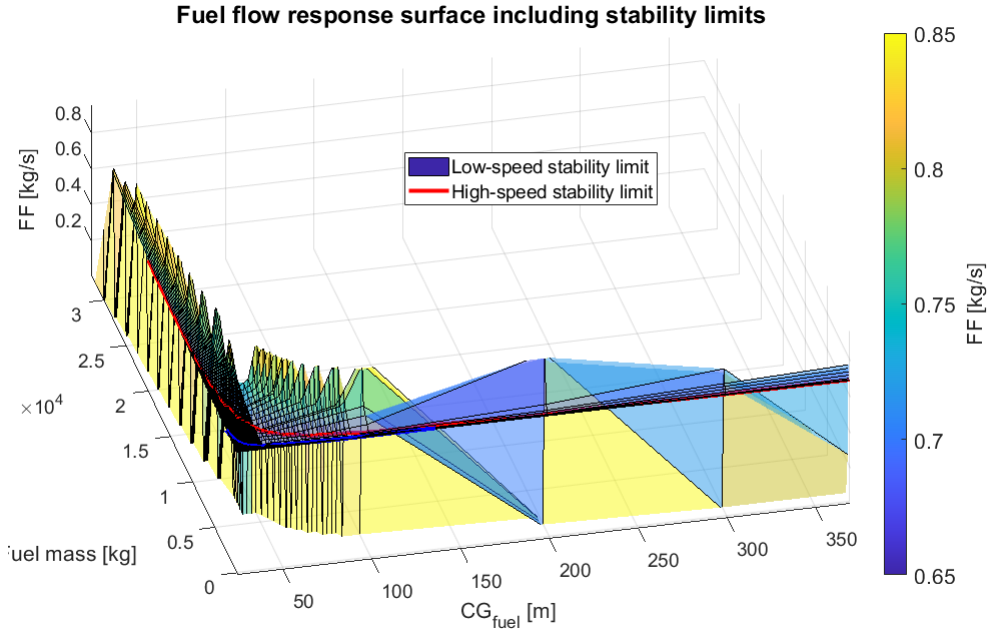

Figure 3.14: 3D fuel flow response surface, showing the fuel flow for different fuel masses and fuel CG combinations, including low- and high-speed stability limits, focusing on the physically infeasible portion and undulations near the edges of the domain.

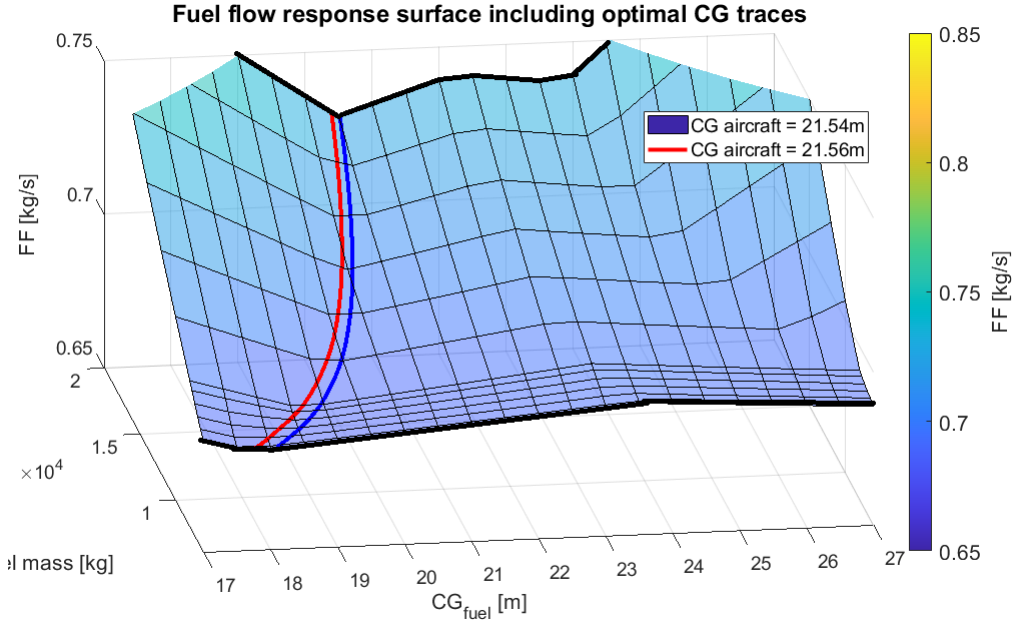

Figure 3.15: Fuel flow response surface for finding the optimal CG.

Table 3.4: General characteristics of PrP fuel system designs.

Characteristic	Design 1	Design 2	Design 3	Design 4
Code	1:11NFF	2:11NFC	3:11YFC	4:21YRF
No. tanks front wing	1	1	1	2
No. tanks rear wing	1	1	1	1
Forward trim tank	No	No	Yes	Yes
Feed cell	Front wing	Front wing	Front wing	Rear wing
Transfer route	Fuselage	Connecting element	Connecting element	Fuselage
Max fuel mass	28464kg	28464kg	28465kg	28466kg

an improved active control of the CG, thereby reducing trim drag and improving the loading flexibility. Here, the design module can be used to create a number of fuel systems, which can subsequently be analysed by the simulation module equipped with the surrogate model to find the fuel burn for any cruise-only flight. This should provide insight in the performance of different designs, and how the layout of the box wing is best taken advantage of.

3.5.1. Box wing fuel system performance

For the purposes of this thesis, four different fuel systems have been designed for the box wing aircraft. Their general characteristics are summarised in Table 3.4. The designs will be referred to by their corresponding code, also presented in Table 3.4. The code essentially summarised the data from the table with a string of digits and letters. A breakdown of how the codes are generated is presented in Fig. 3.16. Note that there is a slight difference in maximum fuel mass between the designs. This is because the capacity of the tanks can only be controlled by moving the chordwise and spanwise limits of the tanks in the .json files. The limits were defined to 3 decimal places, at which point the ParaPy platform no longer had the precision to find differences in the tank size and adding a 4th decimal place would yield the same volume.

Each fuel system is simulated using three different starting conditions: maximum payload, maximum fuel, and ferry. For the maximum payload mission, the aircraft is willed with the maximum payload of 29260kg, and then filled with fuel until either the tanks are full, or the MTOW is reached. For the maximum fuel mission, the aircraft is filled with the maximum amount of fuel, and the payload is added until either the maximum payload is reached, or the MTOW is reached. For the ferry mission, the aircraft is fueled to the maximum fuel capacity, and no payload is added.

Comparing the fuel system designs in this way should provide insight into how the box wing layout is best taken advantage of. The designs were chosen in such a way that each combination of designs reveals the effect of one of the main design drivers. More specifically, designs 1 and 2 reveal the effect of utilising the connecting element as a transfer route between tanks. Designs 2 and 3 reveal the effect of adding a forward trim tank to the design. Designs 3 and 4 reveal the effects of the feed cell placement, and splitting the forward wing tank.

3.5.2. Effects of aircraft design parameters

In this analysis, the effects of aircraft design parameters on the fuel system performance are investigated. For this, the MMG can be used to create a set of box wing aircraft different from the reference box wing aircraft. By keeping the same fuel system design (i.e. the same .json-file for the design module), and using the simulation module with the surrogate model, the effect of aircraft design parameters on the fuel system performance can be evaluated. The aircraft parameters that were varied are the engine position, wing sweep angle, and tank sizes. Table 3.5 shows the values over which the aircraft design parameters are swept.

Design 2:11NFC was used for its expected sensitivity towards changes in the wing sweep angle, as it uses the connecting elements for fuel transfer. Moreover, the design features no forward trim tank, which is expected to limit its capability to control the aircraft CG in comparison with designs that are equipped with a forward trim tank. Therefore, should the changes in aircraft design mandate a fuel system with more control over the CG, then design 2:11NFC should be most sensitive.

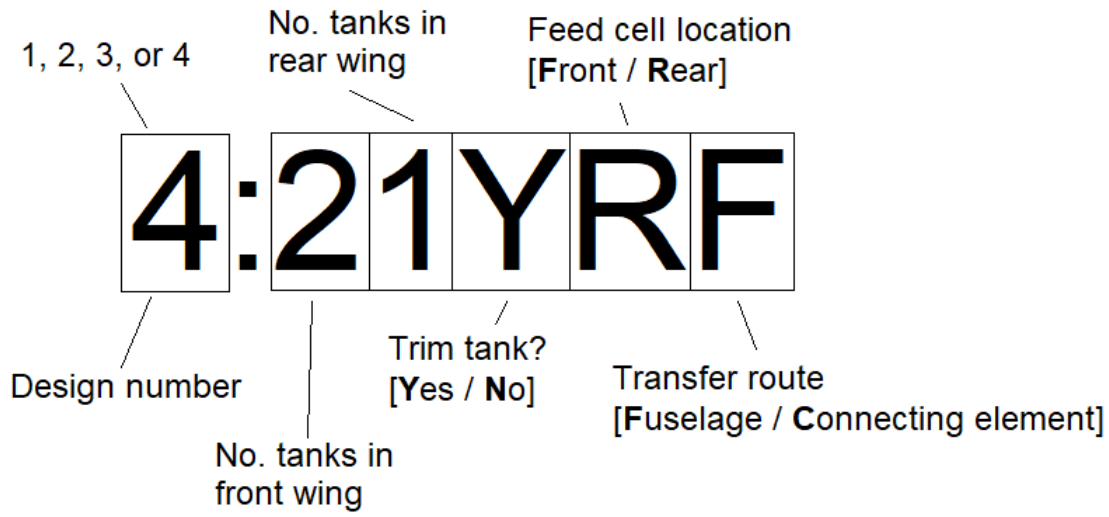

Figure 3.16: Code generation for different fuel system designs. After the double stop, each number or letter represents a design choice.

Table 3.5: Parameters for all design cases.

Parameter	Unit	Lower limit	Upper limit	Step size
Sweep front wing	[deg]	30	50	2
Sweep rear wing	[deg]	10	30	2
Front spar position	x/c	0.2	0.4	0.05
Rear spar position	x/c	0.6	0.8	0.05
Engine position	[m]	32.65	34.55	0.1

It is very important to realise that the instantaneous fuel flow and stability limits for this analysis to be incorrect. Indeed, the surrogate model and stability limits are only valid for the reference aircraft. When the wing sweep angle is changed, it is obvious that there are significant changes in the wing loading and neutral point of the aircraft. This not only means that the surrogate model cannot be used, but also that the direct use of PHALANX would require a new clean aerodynamic database to be generated. Both tasks are very time consuming. Additionally, the changes in the structural wing mass and CG are left unaccounted for, since the mass and inertia database is not updated to reflect the new wing mass and CG.
For the tank size, one must realise that the size is defined by the location of the front and rear spar in the wing, and that the the location of those spars define the available space for the control surfaces. That is, if the aft spar in the wing is moved further aft, the control surface would reduce in size. In this case, the stability limits will move since changing the available space for the control surfaces might change the control surface layout, which in turn changes the stability limits. Additionally, the control-surface database, which is used to determine the trim drag, must be updated. The mass and inertia database would also need to be updated as changing the spar locations will change the structural wing mass and CG. So again, the surrogate model cannot be used, and PHALANX would require an update in its control surface database and mass and inertia database.
Finally, changing the engine position might also warrant the re-evaluation of the clean aerodynamic database, though its influence on the clean aerodynamic database is not as large as a change in the wing sweep angle. Regardless of the aerodynamic effects, it must be noted that changes in the engine position cause a significant change in the aircraft CG, due to their significant mass. While the surrogate model attempts to adjust for this change by using Equation 3.9 to find the surrogate CG, the undulations near the edges of the trimmable domain start to significantly influence the results, especially at low fuel masses.

In all, the fuel flow estimates for these studies are likely to be inaccurate. For the wing sweep angle and tank size analyses, the stability limits will also be inaccurate. The analyses will therefore only provide accurate insight in the system weight, and the interactions between the rear wing size and the rotor burst zone. In absence of the stability limits it can be observed what the effects of the aircraft design parameters are on the aircraft CG at the start of the mission, and to some extend, at the end of the mission.

3.5.3. Comparison with other aircraft

Finally, the effectiveness of the box wing aircraft fuel system is compared against a number of conventional aircraft by evaluating their CG control capabilities. The conventional aircraft, including the F100, A320, and B777, were generated by the MMG, and equipped with a fuel system from the design module. For the conventional data, no data could be found regarding the CG of EOW and payload. The combined CG of the EOW and payload was therefore assumed to lie at 30% of the MAC. For aircraft, it was validated that such a CG results in flight conditions within the flight envelope by checking their respective load sheets.

In order to get a sense for the CG control capabilities, the simulation module was used with the pre-set burn sequence, such that loading diagrams could be generated, wherein the CG envelope in %MAC is plotted for any possible fuel mass. In addition, Equation 3.7 can be used to get a sense for the relative size of the CG envelopes.

4

Verification and validation

This chapter verifies that the design and simulation module work as intended, and validates that their results are representative. In short, the verification is carried out by plotting the amount of fuel in the tanks as a function of time, checking the workings of the active CG control strategy. Next, the simulated and surrogate CG are plotted as a function of time, along with the instantaneous fuel flow to check for the correct trends in the CG disparity. As a final verification step, the surrogate CG trace is plotted on the surrogate model response surface, checking that the fuel flow corresponds with the response surface. Next, the design module weight breakdown is validated against a number of statistical methods predicting the fuel system weight, and a more detailed weight breakdown of a F100 fuel system.

4.1. Verification

The design module, simulation module, and surrogate model were verified by running a maximum range simulation for reference box wing aircraft using fuel system design 4:21YRF (see also Fig. 3.4), with a CG target of $21.55m$ and a bandwidth of $0.02m$. This specific design and CG target was chosen because the results features many modelled aspects, including 1) sufficient complexity between the tanks to verify the CG control algorithm, 2) flight phases wherein different strategies of the control algorithm are used, and 3) a surrogate CG that exceeds the physical limits of the aircraft.
Figure 4.1 shows how fuel is transferred between the tanks during the mission, and the excursion of the aircraft CG. A small sketch is presented in Fig. 4.2 to understand the position of each tank. During phase I, fuel is burned from the feed tank (rearWing1), and since all other tanks are full, there is no additional transfer. At phase II, the CG is at the lower limit of the allowable band since the fuel burn still causes the CG to move forward. To compensate, fuel is transferred from the forward fuselage tank to the tank in the rear wing, which in this case is also the feed tank. During phase III, the feed tank reaches its threshold of 200kg, which triggers the control system to transfer fuel to the feed tank from the tank with lowest sensitivity: frontWing2. Since fuel is now essentially burned from the latter, whose CG lies in front of the CG, the CG slowly travels to the upper band limit, triggering phase IV. Here, the leftover transfer capacity is used to bring the CG forward by transferring to the forward trim tank, and later to frontWing1. Phase V is where all fuel is transferred forward, and the system is no longer capable of keeping the CG within the target band, eventually drifting towards the low speed stability limit.

The sawtooth pattern that is visible on especially the CG plot is a side effect of the time stepping nature of the simulation - it can be amplified or attenuated by increasing or decreasing the step size, respectively. The pattern occurs because the algorithm operates on the edges of the CG band. That is, there are no efforts made to control the CG as long as it inside the CG band. Additionally, any efforts to control the CG will continue for the duration of the time step, even if that means the CG will overshoot the band. Decreasing the time step will decrease the likelihood of such artefacts at the cost of increased computational effort.
Figure 4.3 shows the difference between the surrogate CG and the simulated CG, in combination with

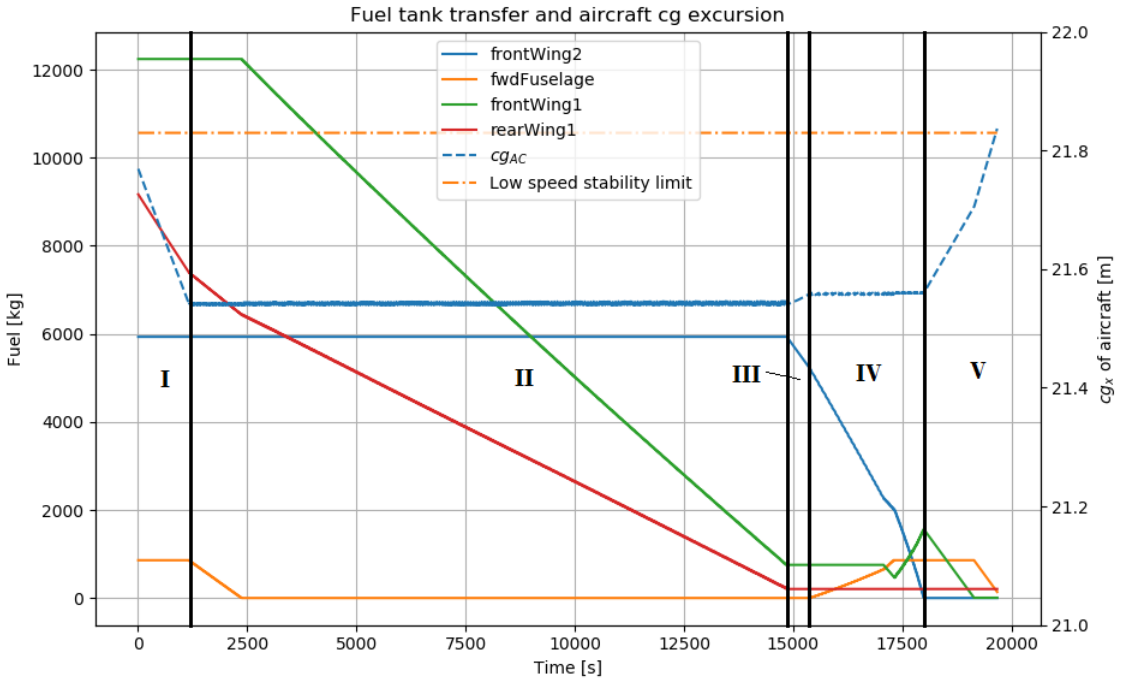

Figure 4.1: Fuel transfer between tanks and excursion of the CG of the aircraft, where full lines correspond to the left axis, and dashed lines correspond to the right axis.

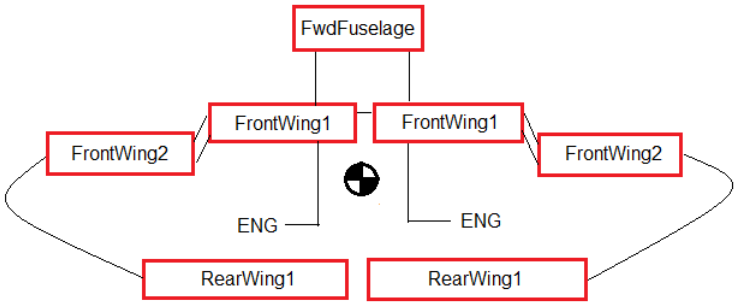

Figure 4.2: Basic sketch of the relative position of the tanks from Fig. 4.1, and the aircraft, also capturing the connectivity between tanks.

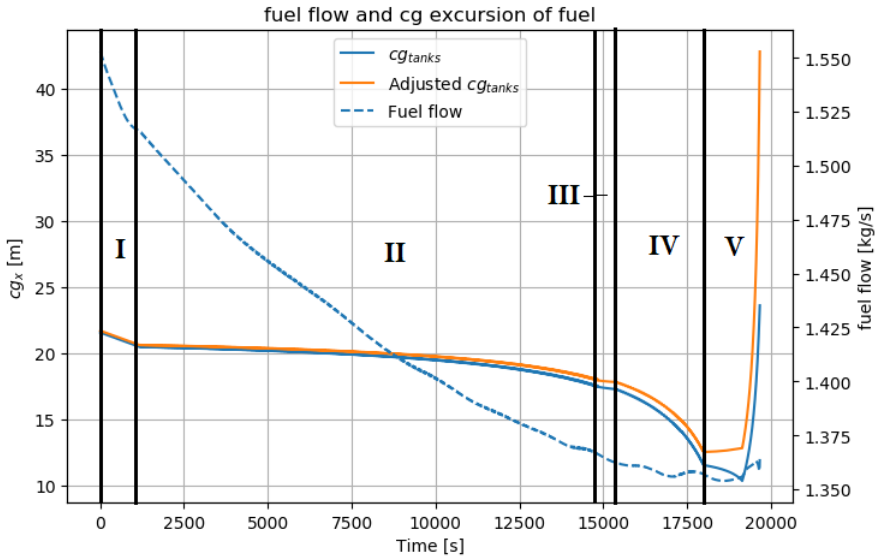

Figure 4.3: Fuel flow and cg excursion of the fuel mass, where full lines correspond to the left axis, and dashed lines correspond to the right axis.

the fuel flow from the surrogate model. Recall from section 3.4.3 that the surrogate CG is a trick to use the surrogate model for aerodynamically similar box wing designs with different mass and inertia databases. From 3.8 and 3.9 it was clear that the absolute difference between the surrogate fuel mass and simulated fuel mass is the same for the complete flight, and that disparity between the surrogate fuel CG and simulated fuel CG is expected to increase. This is because the disparity between the surrogate and simulated aircraft CG (also constant over the flight) must be accounted for by an ever decreasing fuel mass. Indeed, Fig. 4.3 shows that increase in disparity. Additionally, there is a clear decrease in fuel flow over the course of the flight, which is the result of the ever reducing weight of the aircraft as caused by fuel being burnt.

In Fig. 4.4 the curve describing the adjusted fuel CG and fuel flow curve is plotted on the response surface of the surrogate model at maximum payload, where the colour scheme indicates the instantaneous fuel flow. The yellow and green curves indicate the fuel CGs for the low-speed ($21.83m$) and high speed ($22.19m$) stability limits, respectively. The blue curve indicates the surrogate fuel CG trajectory for the simulation from Figs. 4.1 and 4.3. The surrogate fuel CG trajectory is marked with the roman numerals corresponding to those presented in Figs. 4.1 and 4.3. Though hardly visible, the blue trajectory is slightly below the response surface as a result of the disparity in fuel system weight between the reference and simulated aircraft, and this is to be expected.
Comparing the fuel flow from Fig. 4.3 and the fuel CG trajectory from Fig. 4.4 reveals the impact of the ridges on the interpolant. At phase I, there is a slightly sharper decrease in fuel flow due to the CG moving towards the bottom part of the valley corresponding to the optimal CG. This is followed by a smooth decrease in fuel flow in phases II-IV, as the fuel flow is extracted from a region in the response surface with a fine mesh and void of the influence of the ridges. Then, at phase V, the CG trajectory moves sharply to the right, into the region with a coarsened mesh and near the right ridge. The fluctuation that this brings are quite apparent in Fig. 4.3.
In an attempt to be rid of these fluctuations, the results section will also focus on total fuel burn in the time interval of 0-15000s, equating to roughly the first 75% of the flight.

4.2. Validation

A general theme with regard to validation is the lack of publicly available data for modern aircraft. To add to this, Torenbeek [48] notes that weight statements may use different definitions for the same categories, leading to discrepancies between weight statements. In any case, an attempt is made to

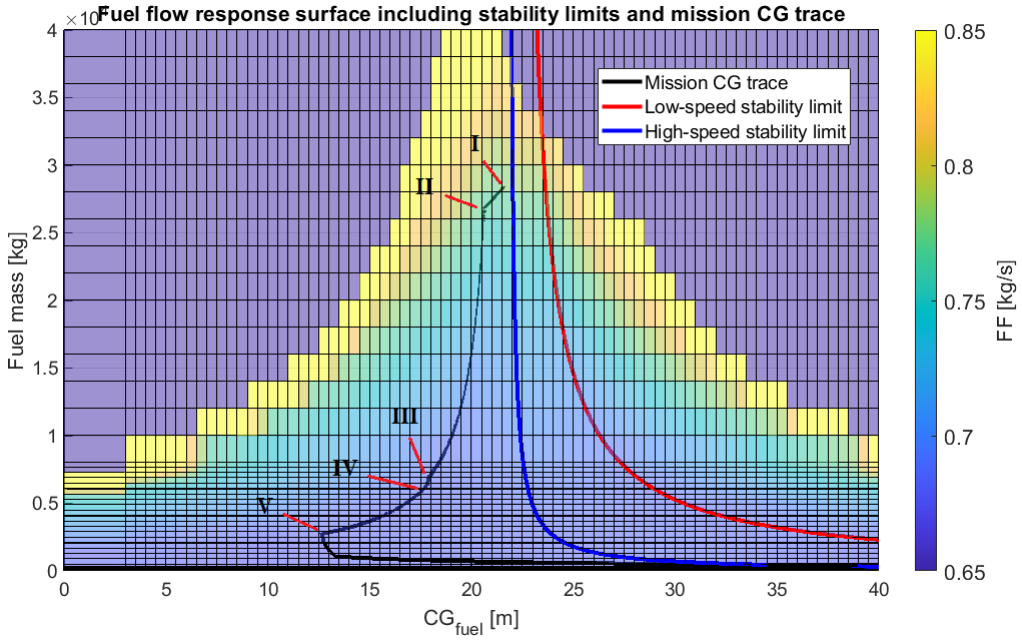

Figure 4.4: Surrogate model response surface for maximum payload, where the colour scheme indicates the instantaneous fuel flow. Black curve indicates the surrogate fuel CG trajectory for the simulation from Figs. 4.1 and 4.3. Blue and red curves represent the low- and high-speed stability limits, respectively.

Table 4.1: Comparison of F100 weight statements from [8] and the module. Entries in **bold** are considered to be the same category. The last row is the total weight of only those components considered by the module. All weights are in kg.

Category	Fokker statement [8]	Module	Error in %
Sealant	90.774	90	-0.85
Pumps	43.88	19.23	-56.17
Distribution	**56.474**	**46.63**	-20.67
Transfer	**2.313**	n/a	n/a
Other	42.53	n/a	n/a
Total	235.97	155.86	-33.95
Total in module	193.44	155.86	-19.42

validate the module by comparing outputs from the module with 1) the weight statement from [8], and 2) statistical methods from [35], [48], and [37].
Table 4.1 shows that the module tends to underestimate the weight of the components, with the exception of the sealant, whose weight was calibrated using the data point from [8]. One possible reasoning is that the module created a simplified, preliminary fuel system that does not capture bolts, rivets, clamps, connections, etc., which may all add to the system weight. Another reasoning is that [8] lacks any definition regarding the weight statement, and so it is impossible to determine exactly which part is put under which category. This problem is even true for the total system weight, since for example fuel flow indication systems and electrical components do not seem to be considered part of the fuel system in [8], while they are included in the weight breakdown reported in [27]. Regardless, if one assumes that the distribution and transfer categories equal the combined fuel line, valve, and nrv weight from the design module, the module still underestimates the total weight by 19% when only considering parts created in by the module. It must be noted, however, that parameters such as the linear mass density of the fuel lines are easily adjusted, possibly resulting in drastically different weight statements.

Table 4.2 compares weight statements generated from the module with statistical methods from [35], [48], and [37]. Strikingly, only Raymer appears to yield a result that is reflective of the size of the aircraft, but grossly underestimates the Fokker's weight. The other statistical methods find little difference in the weight between the B777 and A320 systems despite the significant difference in volume. In

Table 4.2: Comparison of total system weight between statistical models and the module. Reported weights in kg.

Method	B777	A320-200	F100	Box wing
Module	295.31	193.84	155.41	311.09-406.39
Raymer [35]	497.82	241.23	129.73	269.31
Torenbeek [48]	514.07	495.70	321.35	462.28
Beltramo [37]	282.60	280.53	136.37	228.31
Fokker statement [8]	n/a	n/a	235.97	n/a

Table 4.3: Inputs used by statistical methods

Method	No. tanks	Tank volume	Wing length	No. engines
Raymer [35]	Yes	Yes	No	No
Torenbeek [48]	Yes	Yes	No	Yes
Beltramo [37]	Yes	No	Yes	No

all, there is little agreement between the statistical models and the module, and it is difficult to find any indicative trends, aside from the fact that Torenbeek overestimates the system weight in comparison to the other methods. Also note that the statistical methods are aimed at conventional aircraft and cannot distinguish the box wing aircraft, as is reflected by the inputs they use, summarised in Table 4.3.

5

Results

This chapter discusses the data produced by the design and simulation model in light of the design of experiments from section 3.5. First, the CG control capabilities of the box wing aircraft are assessed by comparing the loading diagrams and mean CG ranges of the box wing aircraft with three reference aircraft. Next, the box wing aircraft fuel system designs are assessed on their weight and fuel burn for a complete flight. Finally, the effects of aircraft design parameters on the box wing aircraft fuel system is investigated by analysing system weight, interactions with the rotor burst zone, and the initial and final CG of a maximum fuel mission.

5.1. Loading diagrams

Figures 5.1 and 5.2 plot the loading diagrams for the reference and box wing aircraft. To obtain the loading diagrams, two pre-set sequence simulations were performed. Both simulations start with the maximum amount of fuel, after which payload is added until the MTOW is reached. One simulation will continuously burn fuel from the tank with the fuel CG that lies most aft, while the other continuously burns fuel from the tank with the fuel CG that lies most forward. Consequently, the area enclosed by the two curves represents the mean CG range from Eq. 3.7. Design 1:11NFF is omitted from the figures since its loading diagram is indistinguishable from the plots for design 2:11NFC, as their tank layouts are the same.

Figure 5.1 shows the loading diagrams for designs 2-4 for the box wing aircraft. At the maximum fuel load it is observed that although the capacity is the same for the designs, their CG is different. Design 2:11NFC has the most aft CG as it has no front trim tank like the other designs. Meanwhile, the CG of design 3:11YFC lies forward to the CG of design 4:21YRF because the splitting of the front wing forces the fuel mass outboard and aft due to the sweep angle. Decreasing the gap between the inboard and outboard tanks will decrease this effect. As fuel is burned and space starts to free up to move fuel around, the same outboard front wing tank, however, causes design 4:21YRF to be capable of moving the CG forward of the CG of design 3:11YFC. This phenomenon is especially prevalent at fuel capacities of 10000kg to 16000kg, and may add up to $0.5\%MAC$ in that flight phase. Overall, the forward trim tank in designs 3 and 4 allows one to move the CG forward by roughly $0.8 - 2\%MAC$, depending on the fuel load.

On the other side of the spectrum is the capability to move the CG aft. Design 3:11YFC is least capable of doing so, since the rear wing tank is shrunk in size due to the front trim tank and the desire to keep the capacity the same for all designs for the analysis of the weight and fuel consumption of the designs. In reality, however, there is no reason for the rear wing tank to shrink once a forward trim tank is installed. Therefore, the inability of design 3:11YFC to move the the CG aft is an artefact of the choices made in the design of experiments - its performance should be similar to design 2:11NFC. The split front wing tank of design 4:21YRF, however, is no artefact. The ability to burn fuel from the forward-placed root of the wing causes a significant increase in the ability to move the CG aft, namely $0.3 - 3\%MAC$, depending on the fuel load. That said, the stability limits reveal that the capability to move the CG aft is irrelevant for this particular box wing aircraft. In fact, most efforts made to move

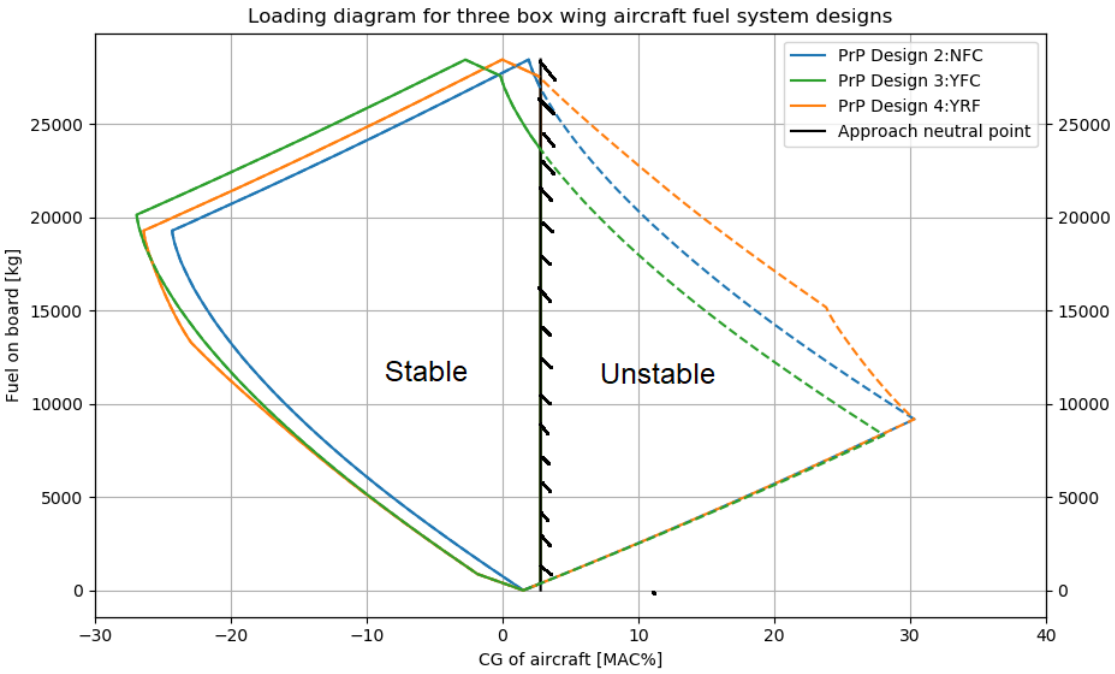

Figure 5.1: Loading diagram for three different box wing aircraft fuel systems.

the CG aft will result an unstable aircraft, and it therefore does not make use of designs aimed at being able to move the CG aft.

Figure 5.2 shows the loading diagrams for three conventional reference aircraft. In reality, these aircraft are not equipped with a trim tank in the empennage, but the design module was used to add trim tanks anyway, in order to understand its effects on the mean CG range. These trim tanks make up roughly 4% of the total fuel capacity. Figure 5.2 shows that the trim tank significantly increases the mean CG range of all conventional aircraft. For all aircraft, the CG can be moved roughly $5\%MAC$ more aft for virtually all fuel loads. Moreover, this increase in CG range falls within the flight envelopes of the aircraft.

Table 5.1 summarises the mean CG ranges for the different box wing aircraft designs and the three reference aircraft. Recall that the mean CG range is computed using Eq. 3.7 and effectively represents the enclosed area in the loading diagrams. Table 5.1 reports two mean CG ranges for each box wing fuel system design: one where stability is disregarded, and one where stability is taken into account. In general, the CG range is reduced by 40% if only the stable region is taken into account. Despite this significant reduction, the box wing aircraft still matches the mean CG ranges of the reference aircraft equipped with trim tanks.
Table 5.1 also reveals that when only the stable region is taken into account, the splitting of the front wing is detrimental to the mean CG range. Indeed, upon closer inspection of Figure 5.1, one will see that at high fuel loads design 3:11YFC is capable of moving the CG more forward than design 4:21YRF, and that this outweighs the advantage that design 4:21YRF has in the fuel load range of 10000kg to 16000kg. The differences between design 2:11NFC and designs 3 and 4 also reveal that adding a forward trim tank to the box wing aircraft increases the mean CG range by $12 - 15\%$ when only considering the stable region. This is in contrast to the reference aircraft, which triple their mean CG range when a trim tank is added.

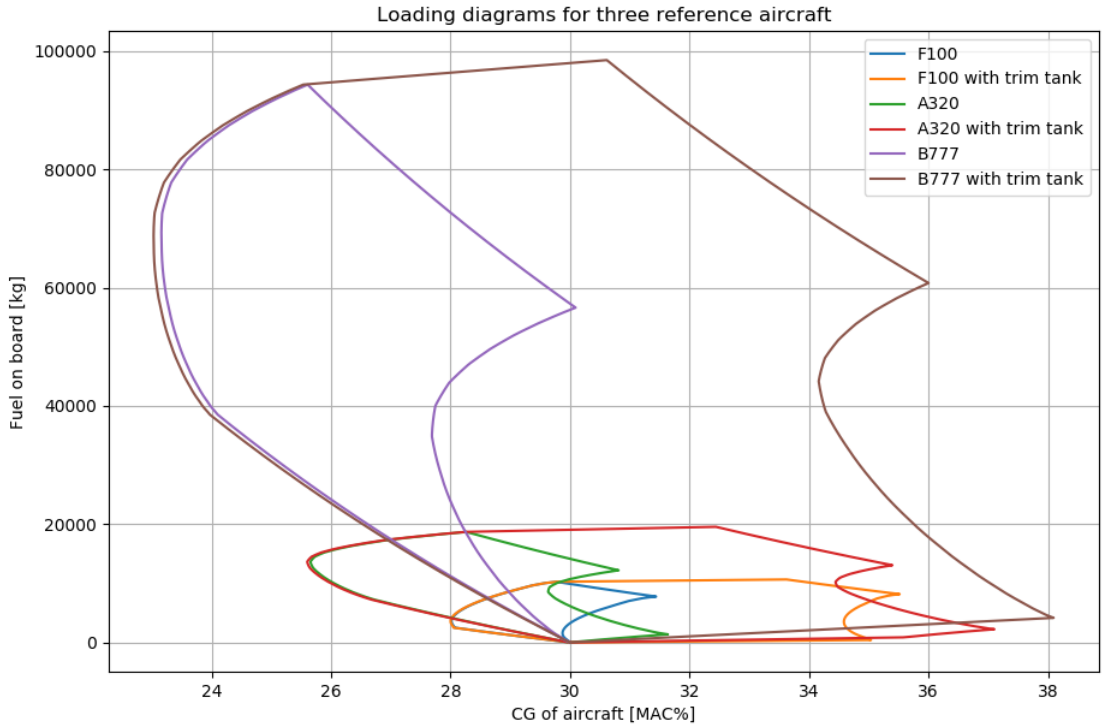

Figure 5.2: Loading diagram for three reference aircraft.

Table 5.1: Mean CG ranges for the PrP and reference aircraft, considering different fuel system designs, and including or excluding the CG region outside the flight envelope.

Aircraft	Box wing			F100		A320		B777	
Fuel system design	Design 2	Design 3	Design 4	No trim	Trim	No trim	Trim	No trim	Trim
$\widehat{CG}$, excl. unstable	8.13	9.363	9.16	1.72	5.91	3.00	7.62	3.22	9.48
$\widehat{CG}$, incl. unstable	14.10	14.30	16.17	-	-	-	-	-	-

Table 5.2: Weight breakdown for the PrP fuel systems.

Component	Design 1:11NFF	Design 2:11NFC	Design 3:11YFC	Design 4:21YRF
Sealant	187.73	187.73	190.2	210.7
Lines	77.87	59.87	72.81	68.38
Pumps	19.01	19.03	25.28	32.10
Valves	22.66	22.66	24.72	28.84
NRVs	2.28	2.28	2.28	4.56
Total	309.55	291.59	315.29	344.68

5.2. Design masses

Table 5.2 shows the weight breakdown of the PrP fuel system designs. Designs 1:11NFF and 2:11NFC reveal that it is preferred to connect the the front and aft wing tanks through the connecting element in terms of system weight. The requirement to have double-walled piping in the pressurised fuselage is too large a penalty to justify running the fuel lines through the fuselage, resulting in a system weight difference of 20kg. This is despite the fact that all tanks are placed inboard, meaning that when they are connected through the connecting elements, the total length of the fuel lines increases. That said, there is an additional design effort to be made when running the fuel lines through the connecting element, as the lines will run through the burst zone of the engine. This imposes a requirement on the fuel lines to be protected by other structural elements in order to reduce the chance of leakage in the event of rotor burst, but does not necessarily add weight. Adding a forward trim tank (design 3:11YFC) to the system increases the weight of the system by 25kg, equating to 8% of the system weight, with respect to design 2:11NFC. The additional fuel lines running through the fuselage in particular contribute a significant portion to this weight increase. Finally, splitting the front tank (design 4:Y21RF) increases the weight by 30kg, equating to 9% with respect to design 3:11YFC. Here, 20kg of the weight increase is contributed by the additional sealant. Notably, the fuel line weight is decreased by placing the feed cell in the rear wing.

5.3. Mission analysis

In this section, the simulation module will use the surrogate model and active CG control to perform cruise-only mission with the four box wing aircraft fuel system designs. More specifically, three missions will be simulated: 1) a ferry mission, 2) a maximum range mission, and 3) a maximum payload mission. The analysis will focus on the CG of the aircraft throughout the mission. The maximum range and payload missions will also investigate the fuel consumption in the first 15000s of the flight.

5.3.1. Ferry mission

Figure 5.3 shows the excursion of the aircraft CG for the ferry mission for all fuel system designs. It becomes clear that every design starts and ends at a CG that is beyond the low-speed stability point, i.e. the stability point for takeoff and landing. Indeed, the uniformly distributed payload reported in [7] has a CG forward of the one corresponding to the empty operating weight of the aircraft, and therefore has a stabilising influence. Without the payload, the fuel system does not have enough authority over the CG to remain in the stable region. In order to achieve stability for a ferry flight, one would need a ballast of roughly 2200kg placed at $x = 5m$, i.e. 5m aft of the aircraft's nose. It is not uncommon for aircraft to require a ballast for ferry flights, the MD-11 being a notorious example of requiring large amounts of ballast fuel during ferry flights. Since civil aircraft are not intended to perform many ferry missions, such missions will not be investigated further.

5.3.2. Maximum range

Figure 5.4 shows the CG excursion of the aircraft and the fuel flow for all designs for the maximum range mission. In the figure, full lines correspond to the left vertical axis and represent the CG of the aircraft, and dashed lines correspond to the right vertical axis and represent the fuel instantaneous fuel

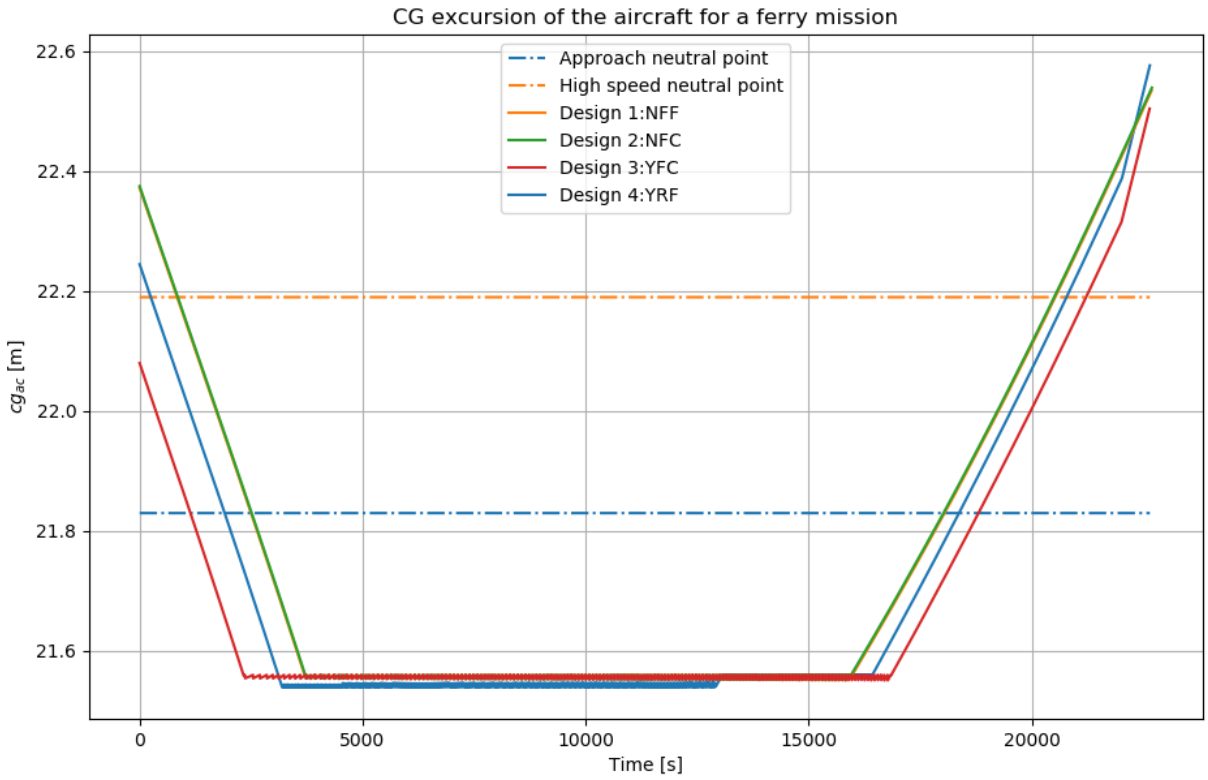

Figure 5.3: CG excursion of aircraft for a ferry mission.

consumption. Quite unsurprisingly given their similarities, the traces of design 1:11NFF and 2:11NFC are indistinguishable, with their total fuel consumption at t=15000s at 21508.8kg and 21509.0kg, respectively. Designs 1:11NFF and 2:11NFC are also the only two designs to be unstable at the start of the flight, entering the stable region at t=120s and t=130s, respectively. On the other hand, designs 3:11YFC and 4:21YRF both start the flight in the stable region, and at t=15000s have consumed 21496.5kg and 21510.4kg, respectively. All designs inch toward instability in the latter stages of the flight. Design 4:21YRF is the only design to become unstable at the end of the flight at t=19780s.
The initial phase at t<1500s is the only moment in time where a noticeable difference in fuel consumption between the designs can be found. Increases in fuel consumption are related to the capability of the designs to quickly reach the optimum CG. Design 3:11YFC starts closest to the optimum CG and also is the first to reach it. Likewise, design 3:11YFC also boasts the lowest fuel consumption at the initial phase of the flight. Design 4:21YRF also has a noticeable advantage over designs 1:11NFF and 2:11NFC in the initial phase of flight, which can also be related to the ability to quickly reach the optimum CG. Despite this initial advantage, design 4:21YRF loses its advantage before t=15000s is reached. Recall that the optimum CG band spans from $21.44m < x < 21.46m$ and that the CG control algorithm causes the aircraft to generally operate on the edges of this domain. Since design 4:21YRF is the only design to split its front wing, it will operate at the lower bound of $21.44m$ for $1100s < t < 14900s$, until the outboard front wing tank is empty. After t=14900s, the fuel is transferred from the inboard front wing tank to the rear wing tank in order to feed the engine from the rear wing tank. At this point in time, the aircraft will operate at the upper bound of $21.46m$ until it is no longer capable of doing so. As was explained in section 3.4.4, the optimum CG lies at $21.45m$, and there may be slight differences between the upper and lower bound of the CG range. It appears that in this case the lower bound is slightly less efficient than the upper bound.

5.3.3. Maximum payload

Figure 5.5 shows the fuel flow and CG excursion of the aircraft for all designs for the maximum payload mission. In the figure, full lines correspond to the left vertical axis and represent the CG of the

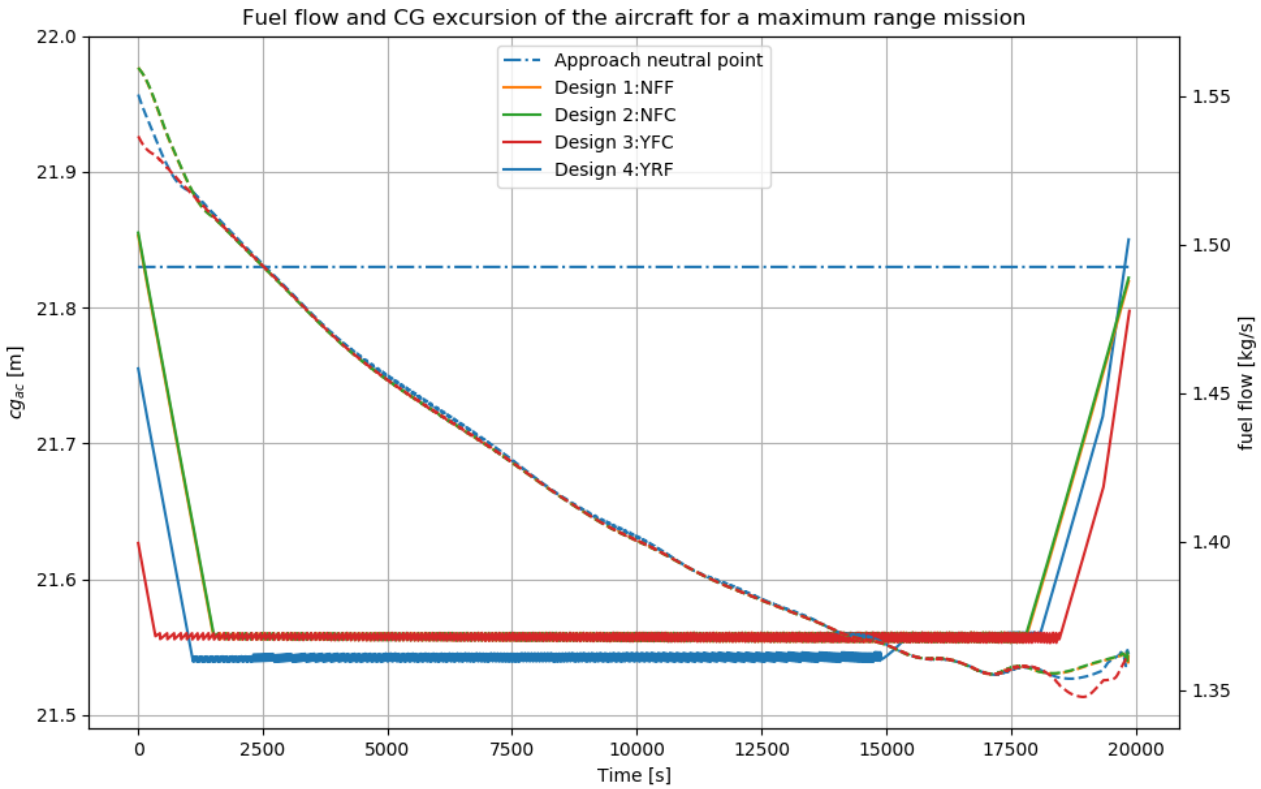

Figure 5.4: Fuel flow and CG excursion of aircraft for a maximum range mission. Full lines correspond to the left vertical axis, indicating the CG of the aircraft. Dashed lines correspond to the right vertical axes, indicating the instantaneous fuel flow.

aircraft, and dashed lines correspond to the right vertical axis and represent the fuel instantaneous fuel consumption. Again, the traces of design 1:11NFF and 2:11NFC are indistinguishable, with their total fuel consumption at t=15000s at 21497.8kg and 21497.9kg, respectively. The keen eye will will see that designs 1:11NFF and 2:11NFC are initially not able to reach the target CG, which is reached at t=455s and t=465s, and then departed at t=16290s and t=16940s, respectively. Designs 3:11YFC and 4:21YRF both reach the CG target at t=25s, and depart the CG target at t=17600s and t=17190s, with their fuel consumption at 15000s at 21497.6kg and 21500.7kg, respectively.
Since the payload has a CG forward to the CG of the aircraft at empty operating weight, and more payload is present than for the maximum range mission, all designs are quick to reach the target CG. In fact, there is no significant difference in fuel consumption between designs 1-3. The increase in fuel consumption of design 4:21YRF can once again be explained by the aircraft operating at the lower CG target limit, where the other designs operate at the upper CG target limit.
The stabilising effect of the payload also ensures that none of the designs become unstable at the end of the flight. Regardless, design 4:21YRF is most unstable at the end of the flight, regardless of the mission. Recall that design 4:21YRF has its feed tank in the rear wing, and that the feed tank fuel load may never drop below 200kg. With decreasing amounts of fuel present in the later stages of the flight, this 200kg starts to constitute a significant portion of the remaining fuel and will act as a destabilising ballast, causing design 4:21YRF to become comparatively unstable.

5.4. Aircraft design parameters

Until this point, the results have been based on the reference box wing aircraft from [7]. Therefore, the aerodynamic, and mass and inertia databases have been representative of the aircraft. In this section, however, the box wing aircraft design parameters are altered. Consequently, the aerodynamic, and mass and inertia databases are no longer valid (see also section 3.4.3). The point of this section is to analyse how the fuel system changes as a result of changing the aircraft design parameters. This analysis will disregard the fuel consumption, since these figures are likely to be inaccurate. Instead, the

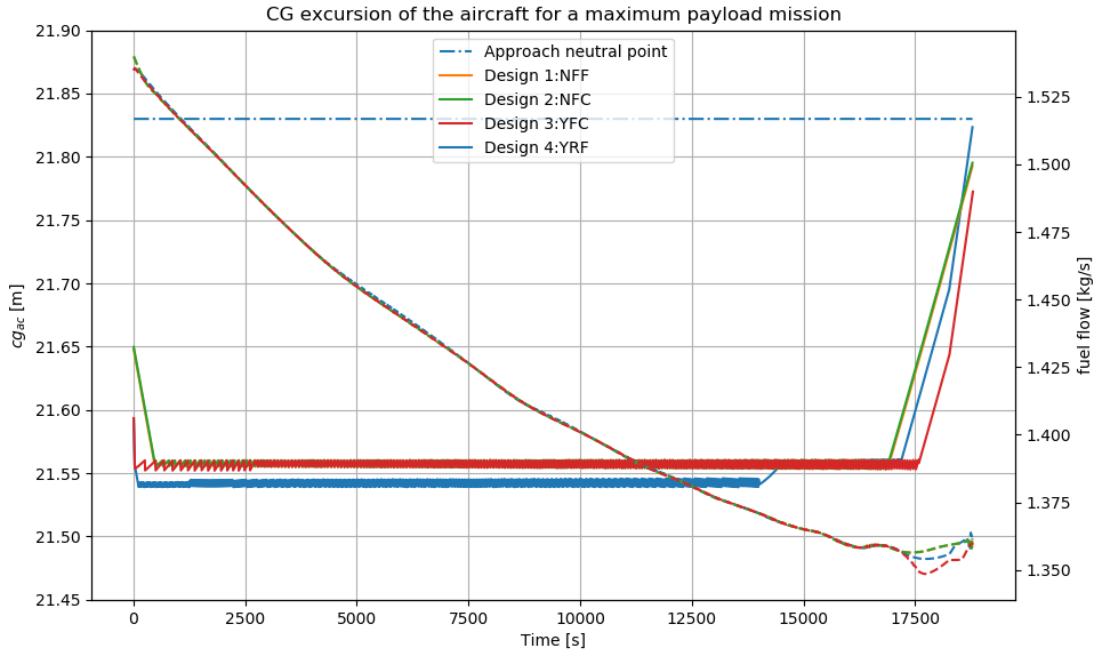

Figure 5.5: Fuel flow and CG excursion of the fuel for a maximum payload mission.

focus will lie on how the fuel system geometry changes, and how this affects the ability to keep the CG of the aircraft forward. The previous sections have shown that this is particularly important at the start and end of the flight. All analysis are performed using design 2:11NFC, for its expected sensitivity to the changes. The focus is also on the maximum range missions, since these best reflect the changes in the fuel capacity, and are more prone to instability due to the decreasing amounts of stabilising payload.

5.4.1. Engine position

Figure 5.6 shows the CG trajectories of the aircraft for different engine positions for the maximum range mission. As a general rule for the end of the mission, when the engine is placed more aft, the CG will start to drift from the target CG at an earlier point in time. Hence, moving the engine forward will improve the stability and the ability to maintain the target CG at the end of the mission. For a maximum range mission, moving the engine forward from 33.65 to 32.65m delays the CG target departure from t=18310s to t=20510s.

At the start of the mission, the effect of the engine placement is dependant on the mission. When considering a maximum range mission, one does not have the luxury to move fuel around, as the tanks are always full. Consequently, the shift in rotor burst zone (i.e. the allowable region for the fuel tank in the rear wing) and shift in engine placement dominate the changes in the initial CG. The interaction between the rotor burst zone and rear wing tank size is depicted in Figure 5.7. The combination with Fig. 5.6 reveals that the increase in the rear wing tank size outweighs the effect of the engine moving forward - the initial CG moves aft when the engine is moved forward. Moving the engine forward from 33.65m to 32.65m increases the initial CG from 21.95m to 22.06m and delays the achievement of the CG target from t=2040s to t=2645s.

Conversely, for a maximum payload mission, there is room to decide on an initial fuel distribution, allowing more control over the initial CG. Here, the effect of the engine is reversed with respect to the maximum range mission; moving the engine forward increases the aircraft's capability of placing the initial CG at the target CG. At $x_{eng} > 33.13m$ the engine is too far aft for the fuel system to move the CG forward enough to immediately achieve the target CG. However, at $x_{eng} < 33.15m$ the fuel system must work to move the CG aft, and since the effect of a 'growing' rear wing tank is larger than the engine moving forward, the fuel system will have no problem placing the initial CG at the target CG. Moving the engine forward from 34.14m to 33.15 allows one to achieve the target CG at t=790s, and t=105s, respectively.

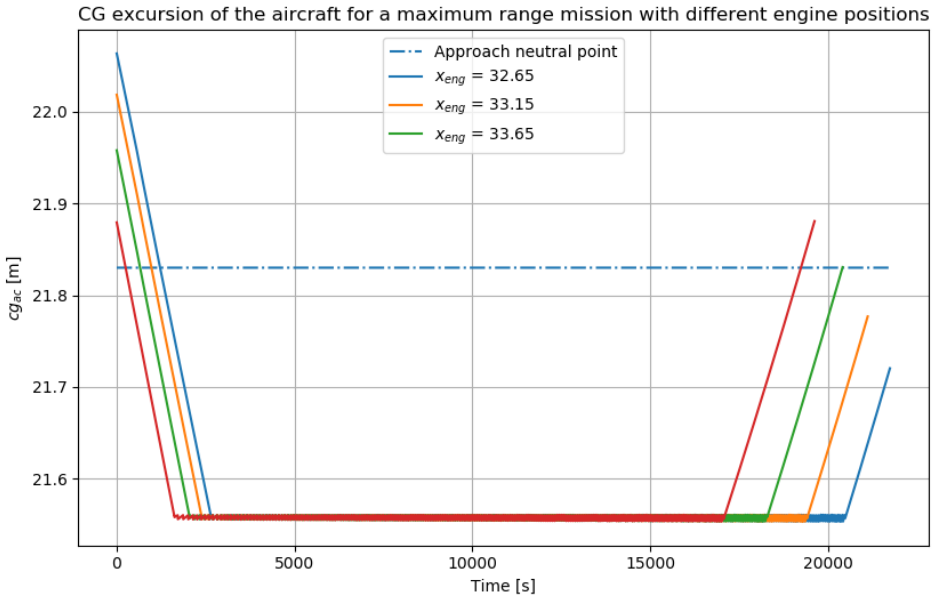

Figure 5.6: CG excursion of the aircraft for a maximum range mission for different engine positions.

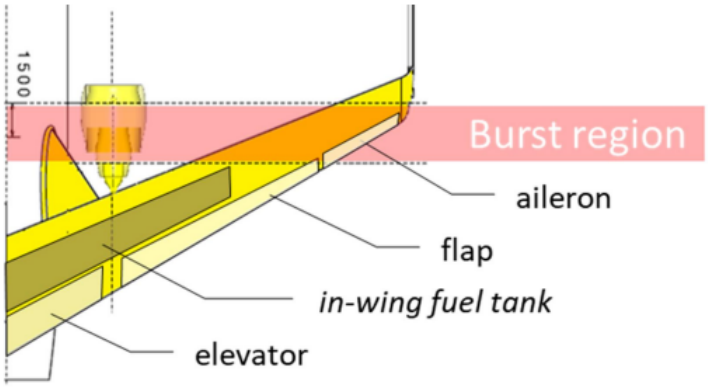

Figure 5.7: Interaction between the rotor burst zone and the wing tank size [7]

5.4.2. Sweep angle

Figure 5.8 shows the excursion of the CG of the aircraft for maximum range missions with different sweep angles for the front and rear wing. As discussed in section 3.5, the front and rear wing are changed independently: when the front sweep angle is changed, the rear wing sweep angle is kept at its original sweep angle, and vice versa. There are two observations to be made for Fig. 5.8: 1) At the start of the mission the rear wing sweep angle has more effect on the CG of the fuel than the front wing sweep angle, and 2) changing the rear sweep angle affects the range of the aircraft, but not the final CG of the fuel.

The first observation may sound counter intuitive, as the front wing tank is generally larger than the rear wing tank, and would therefore have a larger influence on the CG. However, one must not forget that the rear wing tank is bound by the rotor burst zone. Therefore, decreasing the sweep forward not only moves the CG of the fuel (system) aft, but also increases the rear wing tank size. The edge case here is that a decrease in sweep forward from 20deg to 10deg results in a similar shift in CG of the fuel as an increase in sweep back from 40 to 50, because the rear tank is not enlarged as much at low sweep forward angles since most of the wing remains outside the rotor burst zone.

The second observation is also in part explained by the enlargement of the rear wing tank, as the range is obviously increased as the system's capacity is increased. The rear sweep angle does not affect the final CG of the fuel because of the choice in feed cell location - the rear wing is empty at the final phase of the mission and therefore does not affect the CG of the fuel anymore. It is expected that placing the feed cell in the rear wing will cause the sweep angle to have a relatively small influence on the final CG. Regardless, there is a significant difference in the final CG of the aircraft caused by changes in the fuel system weight and CG due to the sweep forward. The difference being a change in system CG from 20.92m to 22.54m, and in system weight from 283.66kg to 308.67kg for 30deg sweep forward and 10deg sweep forward, respectively. As a side note, the difference in rear tank size between the two is 13302kg at 10deg sweep forward, and 8135kg at 30deg sweep forward.

Again, these observations are made without considering the effects of changes in the structural weight of the wings, and changes in the stability limits. The author expects the first observation to hold true in the face of changes in the structural weight of the wings, since the analysis for the engine position has shown that changes in the rear wing tank size overcome even large changes in the CG of the empty aircraft, such as changing the engine position. The author, however, is unsure if the second observation hold when the wing weight is considered. Likewise, the changes in the stability limits and optimal CG due to changes in the wing loading may counteract any gains made towards stabilising the aircraft using the fuel system.

5.4.3. Spar locations

As is the case for the sweep angles, the front and rear spars in the front and rear wing were moved independently of each other during the parameter sweeps. Doing so changes the control surface sizing, and therefore the stability limits and optimal CG might not be reliable. Despite these unreliable data points, it is again to be expected that for a maximum range mission, the added fuel capacity will dominate the CG change - moving any spar aft will move the CG aft, and vice versa. It must also be noted that changes in the front wing spars cause significant changes in the capacity of the fuel system, to the point where there is insufficient capacity to reach the MTOW of the aircraft. Moving the front wing front spar from $0.35x/c$ to $0.3x/c$ reduces the front wing tank capacity from 19290kg to 16735kg. The end of the mission can be discussed only in isolation of other effects, since there is a fine balance between two effects: changes in the system CG, and changes in the fuel CG. In most cases, moving a spar forward moves the CG of the aircraft at the end of the flight forward. The exception to this rule is the front wing aft spar. Moving this spar aft from $0.7x/c$ to $0.75x/c$ moves the system CG forward from 21.56m to 21.39m due to the increase in tank size, while the CG of the fuel is moved aft from 12.47m to 12.66m. As the weight of the fuel and fuel system are in the same order of magnitude at the end of the flight, the effects cancel, and no significant change in the CG of the aircraft is observed.

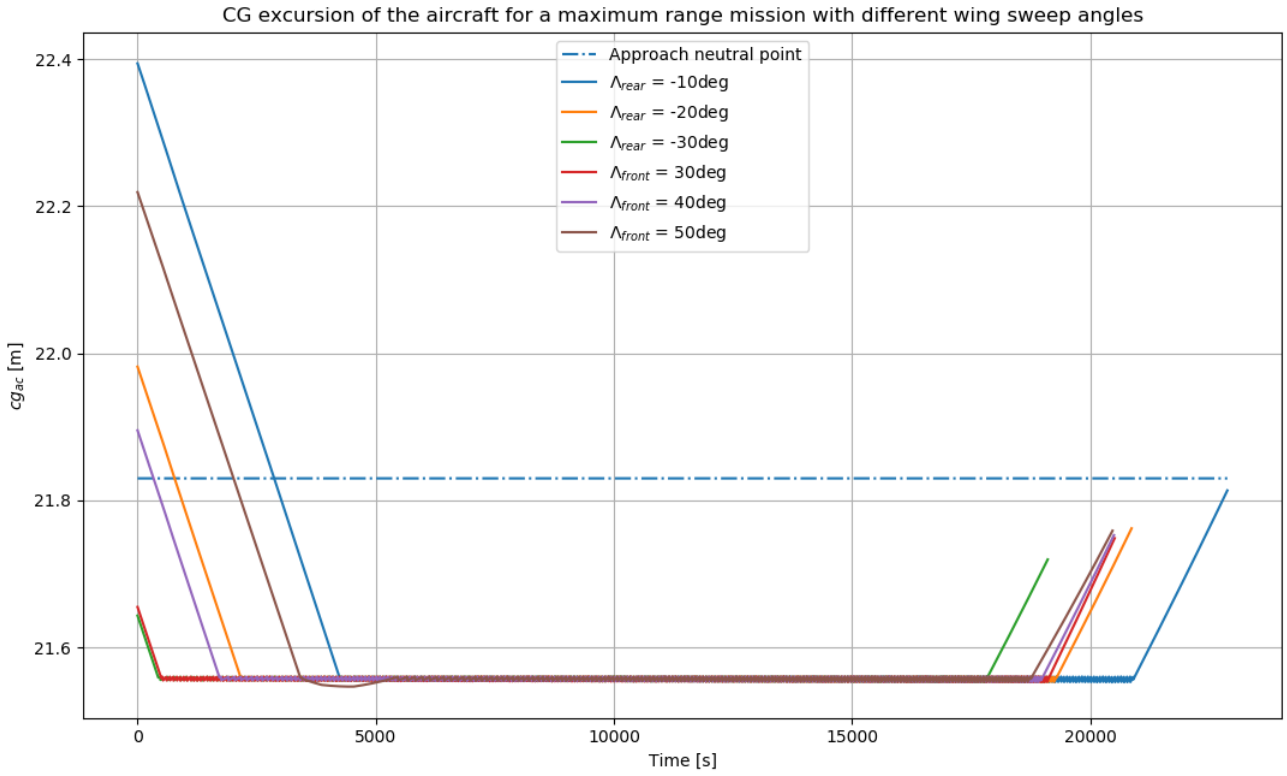

Figure 5.8: CG excursion of the fuel for a maximum range mission for sweep angles.

6

Discussion

The attentive reader will have noticed that the shaft power off-take has not been included in the results, despite being included in the methodology. This is because plugging the corrects values has proven to be a real challenge. Indeed, Table 3.2 heavily relies on the expertise of the designer to estimate the correct values beforehand. Despite the author's best efforts, the module seems to consistently underestimate the power off-take of the pumps. It was possible to verify this using data sheets such as [49], which is in fact used in one of the reference aircraft. Still, Langton *et al.* [5] note that values for the friction penalty K may vary from 0.3 to 6 for a non-return valve, which makes it difficult to estimate the friction losses this early in the design stage. An initial investigation into the the equivalent fuel burn due to the pump power off-take revealed that this was insignificant compared to the difference in total fuel burn due to changes in the aircraft CG (0.02kg).

Regardless of the module's underestimation of the pump's power off-take, it was observed that the general trends for pump power and weight are ostensibly correct. For example, the pump weight would increase if the height difference between the pump and destination increased, albeit that the increase was very slight. Since the pump's power is grossly underestimated, the pump weight is mostly comprised of the installation penalty from Fig. 3.6. Consequently, module's sensitivity towards pump weight increases due to power off-take is virtually zero, while the relative sensitivity towards pump weight increases due to system complexity (i.e. adding more pumps) is increased.

The module also encounters further issues when estimating the weight of the fuel system. Though the weight estimations for the sealant and pump weight feature physics-based methods to find their edge length and power requirement, respectively, they ultimately rely on data fits to translate the edge length and power requirement to system weight. To add to this, there are many more ways to fit data, and many more ways to compute the required physical data presented herein. For example, one might op to fit the tank's surface area or volume to other known tank sealant weights, or fit the flow rate requirement of pumps to the pump's weight, instead of the pump's power requirement. Indeed, it cannot be taken for granted that the data fits presented herein yield the most reliable results.

Regarding the use of the PHALANX surrogate model, one will often see that towards the end of the mission the fuel flow starts fluctuating. It has already been alluded to that this fluctuation is caused by how the surrogate model is fed an adjusted fuel condition in order to compensate for the difference in aircraft design between the aircraft model in PHALANX and the module. From the results it is clear that these fluctuations tend to dominate the aircraft range reported by the module. On the other hand, Fig. 5.4 demonstrates that differences in CG at the start of the mission are captured well enough to distinguish the resulting trends in the fuel flow. At the end of the mission, however, we see that a departure from the target CG quickly results in oscillations that cannot be related to the CG position, even though they are in the stable area. It is possible to develop a hybrid approach that uses the surrogate model during the initial 15000s of the mission, and directly using PHALANX for the final part of the mission. This way, the reduced computational effort of the surrogate model, and the reduced end-of-mission fuel flow fluctuation due to bypassing the surrogate model are both taken advantage of.

The use of the surrogate model also omits any aerodynamic and structural effects from the results. While is it assumed that no aerodynamic effects occur when only the fuel system design is changed,

changing any of the aircraft design parameters will cause aerodynamic effects and demand changes in the structure of the aircraft. Hence both the aerodynamic and mass and inertia database from PHALANX are invalidated. It is possible to capture the changes in both database by replacing them with updated databases. However, creating such databases is particularly cumbersome. Even when such effort is made, it is advised that a new surrogate model is created if one wishes to evaluate many different fuel system designs. Indeed, it is possible to forego the use of the surrogate model and have PHALANX directly evaluate the fuel flow at any point during the mission, but this would significantly increase the computation effort, and greatly reduce the module's effectiveness as a preliminary design tool.

7

Conclusions and recommendations

In an attempt to quantify the expected advantages and disadvantages of the box wing aircraft fuel system, the MMG has been extended with an aircraft type agnostic fuel system module. The module is capable of generating a preliminary fuel system geometry, assessing the weight of different fuel system designs, and estimation the fuel flow for different missions comprised of a single cruise segment.
The results indicate that it is advisable to use the connecting element between the front and rear wing to connect the fuel tanks in the wings, saving up to 6% system weight compared to similar designs where the connection runs through the fuselage. Adding a forward trim tank adds roughly 8% to the system weight and increases the usable CG range by 12-15%. The mean stable CG range for the box wing aircraft equipped with a forward trim tank is comparable to the mean stable CG range of a B777 equipped with a trim tank. Compared to a conventional aircraft, however, the effect of adding a forward trim tank is minor. Even more so, for conventional aircraft there appears to be no consensus on the value of a trim tank, reflected by the fact that a trim tank is not standard equipment. However, the effect of a trim tank in a conventional aircraft is much more pronounced, hence one is led to wonder if a trim tank is warranted for a box wing aircraft, since the added system complexity is similar. Results also indicate that adding a forward trim tank results in an insignificant fuel save of 0.2kg (<0.01%) within the first 15000s (75%) of the mission.
Generally, the box wing aircraft struggles with stability at the start and end of the mission. Ferry and maximum range missions in particular, where the tanks are completely filled, prove to be problematic, as the CG is the stabilising influence of the payload is not as pronounced. In order to achieve a stable ferry flight, a balancing payload of roughly 2200kg must be placed 5m from the aircraft's nose. Adding a forward trim tank relieves the stability problem at the start of the flight, where the CG of the aircraft can be moved by as much as 3% MAC.
The effects of aircraft parameters on the fuel system and the aircraft's balance are mostly dominated by the interaction between the rotor burst zone and the rear wing tank, effects on the fuel system's CG, and placement of the feed cell. Regarding the initial CG, the change in rear wing tank size due to the shift of the rotor burst zone dominated any changes in the CG caused by the system weight or fuel CG shift. At the end of the mission, the size of the tanks is no longer significant. Instead, changes in the final CG are due to the relative changes in system weight and CG, and the placement of the fuel CG. It must be noted that these observations are made in isolation of aerodynamic, mass and inertial changes. It is expected that this does not have much ramifications for the CG at the start of the flight, but changes in aircraft CG at the end of the flight due to the fuel system changes are expected to be dominated by changes in the wing and engine weight, and neutral point changes.
The combination of the weight statements and loading diagrams for the different fuel designs reveals that design 4:21YRF is not an effective solution. Out of the four designs, it is not only the heaviest, but also the most complex, meaning that is it also most prone to failure modes. While its forward trim tank increases its mean CG range with respect to designs 1:11NFF and 2:11NFC, it holds no significant advantage over design 3:11YFC, which is equipped with the same trim tank. Likewise, design 1:11NFF has the same loading diagram as design 2:11NFC, but is heavier, making design 2:11NFC the superior choice between the two. Designs 2:11NFC and 3:11YFC appear to be most effective, where a trade-off must be made between the added start-of-flight stability of design 3:11YFC at the cost of added system

complexity and weight.

Continued efforts towards the fuel system module should focus on reducing the fuel flow oscillations nearing the end of the missions, by either 1) improving the accuracy of the surrogate model at low fuel masses, 2) implementing a hybrid method where PHALANX is directly used to simulate parts of the mission where the fuel mass is low, or 3) sacrificing the reduced computational effort by foregoing the use of the surrogate model and directly using PHALANX to simulate the fuel flow for the complete mission. Alternatively, it is possible to couple the engine map from PHALANX to another simple aerodynamic solver such as AVL, which would allow one to assess the relative significance between changes in trim drag and the neutral point caused by the sweep angle and control surfaces, and changes in the fuel CG and aircraft CG due to the fuel system changes caused by the sweep angle and control surfaces. It should be noted this will not solve the issue of changes in the wing structure, nor is the total trim drag expected to be very accurate. The module can also be further improved by developing and comparing alternative methods for the estimation of the sealant mass and pump sizing. Also, if the geometry model is of sufficient fidelity, the current pump sizing methodology can be replaced by a fluid network analysis. Finally, the model can be improved by developing and comparing alternative methods for the estimation of the sealant mass and pump sizing.
This work may also act as a precedent to a KBE-based approach to preliminary analysis and sizing of a complete set of aircraft subsystems. Other authors have already sized sets of aircraft subsystems, but have mostly made use of low-fidelity simulations. Since this module uses a subsystem agnostic methodology to compute the equivalent fuel burn of a subsystem, it is possible to add more subsystems and increase the understanding of subsystem inter-dependency. In any case, integrating additional subsystems into this approach inherently increases the understanding of space allocation, and, for example, increases the fidelity of the fuel line routing.

Bibliography

[1] R. Lange, J. Cahill, E. Bradley, R. Eudaily, C. Jenness, and D. Macwilkinson, *Feasibility study of the transonic biplane concept for transport aircraft application,* (1974).

[2] D. Schiktanz and D. Scholz, *Box wing fundamentals–an aircraft design perspective,* DGLR Dtsch. Luft-und , 601 (2011).

[3] S. A. Andrews and R. E. Perez, *Comparison of box-wing and conventional aircraft mission performance using multidisciplinary analysis and optimization,* Aerospace Science and Technology **79**, 336 (2018).

[4] A. Frediani, UNIPI, TUD, ONERA, DLR, ENSAM, and SKYBOX, *Parsifal proposal,* (2016).

[5] R. Langton, C. Clark, M. Hewitt, and L. Richards, *Aircraft fuel systems*, Vol. 24 (John Wiley & Sons, 2009).

[6] D. Rajaram, Y. Cai, I. Chakraborty, and D. N. Mavris, *Integrated sizing and optimization of aircraft and subsystem architectures in early design,* Journal of Aircraft **55**, 1942 (2018).

[7] C. Varriale, K. Abu Salem, V. Cipolla, and V. Binante, *PARSIFAL Deliverable 6.2: Design optimization for stability and control of a PrandtlPlane*, Tech. Rep. (TU Delft and University of Pisa and SKYBOX, 2020).

[8] Fokker, *Detail and Group Weight Statement F28 Mk0100 A482*, Tech. Rep. (1994).

[9] A. Bows, *Aviation and climate change: confronting the challenge,* The Aeronautical Journal **114**, 459 (2010).

[10] A. Flightpath, *2050-europe's vision for aviation,* Advisory Council for Aeronautics Research in Europe (2011).

[11] L. Prandtl, *Induced drag of multiplanes,* (1924).

[12] V. Cipolla, A. Frediani, K. Abu Salem, M. Picchi Scardaoni, A. Nuti, and V. Binante, *Conceptual design of a box-wing aircraft for the air transport of the future,* in *2018 Aviation Technology, Integration, and Operations Conference* (2018) p. 3660.

[13] EASA, CS-25, *Certification specifications for large aeroplanes, cs 25,* (2009).

[14] H. Gagnon and D. W. Zingg, *Aerodynamic optimization trade study of a box-wing aircraft configuration,* Journal of Aircraft **53**, 971 (2016).

[15] T. Chau and D. W. Zingg, *Aerodynamic shape optimization of a box-wing regional aircraft based on the reynolds-averaged navier-stokes equations,* in *35th AIAA Applied Aerodynamics Conference* (2017) p. 3258.

[16] P. O. Jemitola, *Conceptual design and optimization methodology for box wing aircraft,* (2012).

[17] S. A. Andrews and R. E. Perez, *Parametric study of box-wing aerodynamics for minimum drag under stability and maneuverability constraints,* in *33rd AIAA Applied Aerodynamics Conference* (2015) p. 3291.

[18] S. Chai, P. Crisafulli, and W. Mason, *Aircraft center of gravity estimation in conceptual/preliminary design,* in *Aircraft Engineering, Technology, and Operations Congress* (1995) p. 3882.

[19] H. Gavel, J. Olvander, and P. Krus, *Aircraft fuel system synthesis aided by interactive morphology, optimization and probabilistic design,* in *46th AIAA Aerospace Sciences Meeting and Exhibit* (2008) p. 159.

[20] D. M. Judt and C. Lawson, *Development of an automated aircraft subsystem architecture generation and analysis tool,* Engineering Computations **33**, 1327 (2016).

[21] D. Pate, M. Patterson, and B. German, *Methods for optimizing a family of reconfigurable aircraft,* in *11th AIAA Aviation Technology, Integration, and Operations (ATIO) Conference, including the AIAA Balloon Systems Conference and 19th AIAA Lighter-Than* (2011) p. 6850.

[22] J. Ölvander, B. Lundén, and H. Gavel, *A computerized optimization framework for the morphological matrix applied to aircraft conceptual design,* Computer-Aided Design **41**, 187 (2009).

[23] L. Boggero, *Design techniques to support aircraft systems development in a collaborative mdo environment,* Turin (IT): Doctoral dissertation (2018).

[24] T. Lammering and E. Stumpf, *Integration of aircraft systems into conceptual design synthesis*, Tech. Rep. (Lehrstuhl und Institut für Luft-und Raumfahrtsysteme (ILR), 2014).

[25] R. Seresinhe and C. Lawson, *Electrical load-sizing methodology to aid conceptual and preliminary design of large commercial aircraft,* Proceedings of the Institution of Mechanical Engineers, Part G: Journal of Aerospace Engineering **229**, 445 (2015).

[26] G. Gilyard and M. España, *On the use of controls for subsonic transport performance improvement-overview and future directions,* in *19th Atmospheric Flight Mechanics Conference* (1994) p. 3515.

[27] C. Kong, M.-c. Kang, C.-h. Lee, and D.-j. Han, *Fuel system design of the smart uav considering operational reliability,* Aircraft Engineering and Aerospace Technology **78**, 204 (2006).

[28] M. Bodie and M. Wolff, *Robust optimization of an aircraft power thermal management system,* in *46th AIAA/ASME/SAE/ASEE Joint Propulsion Conference & Exhibit* (2010) p. 7086.

[29] D. B. Doman, *Fuel flow topology and control for extending aircraft thermal endurance,* Journal of Thermophysics and Heat Transfer **32**, 35 (2017).

[30] P. O. Jemitola and J. P. Fielding, *Box wing aircraft conceptual design,* in *28th congress of the international council of the aeronautical sciences* (2012) pp. 23–28.

[31] R. Elmendorp, R. Vos, and G. La Rocca, *A conceptual design and analysis method for conventional and unconventional airplanes,* in *ICAS 2014: Proceedings of the 29th Congress of the International Council of the Aeronautical Sciences, St. Petersburg, Russia, 7-12 September 2014* (International Council of Aeronautical Sciences, 2014).

[32] C. Varriale and M. Voskuijl, *A control allocation approach to induce the center of pressure position and shape the aircraft transient response,* Aerospace Science and Technology **119**, 107092 (2021).

[33] G. La Rocca, *Knowledge based engineering: Between ai and cad. review of a language based technology to support engineering design,* Advanced engineering informatics **26**, 159 (2012).

[34] ParaPy, BV, *Parapy–knowledge based engineering platform,* (2017).

[35] D. Raymer, *Aircraft design: a conceptual approach* (American Institute of Aeronautics and Astronautics, Inc., 2018).

[36] I. Chakraborty, *Subsystem architecture sizing and analysis for aircraft conceptual design*, Ph.D. thesis, Georgia Institute of Technology (2015).

[37] M. N. Beltramo, D. L. Trapp, B. W. Kimoto, and D. P. Marsh, *Parametric study of transport aircraft systems cost and weight,* (1977).

[38] A. Westenberger *et al.*, *Liquid hydrogen fuelled aircraft-system analysis,* CRYOPLANE, The European Commission, Brussels, Belgium, Report No. GRD1-1999-10014 (2003).

[39] D. Verstraete, *Long range transport aircraft using hydrogen fuel,* International journal of hydrogen energy **38**, 14824 (2013).

[40] A. Raju Kulkarni, C. Varriale, M. Voskuijl, G. La Rocca, and L. L. Veldhuis, *Assessment of sub-scale designs for scaled flight testing,* in *AIAA Aviation 2019 Forum* (2019) p. 3089.

[41] Eaton Aerospace Limited, *Engine Fuel Return Check Valve, Data Sheet*, 21F0010 (2010).

[42] Eaton Aerospace Limited, *Pedestal Ball Valve, Data Sheet*, 12R0078 (2011).

[43] C. Svahn, *Quantified interactive morphological matrix: An automated approach to aircraft fuel system synthesis,* (2006).

[44] M. Cavcar, *The international standard atmosphere (isa),* Anadolu University, Turkey **30**, 1 (2000).

[45] P. Spedding, E. Bénard, and G. McNally, *Fluid flow through 90 degree bends,* Developments in Chemical Engineering and Mineral Processing **12**, 107 (2004).

[46] D. Scholz, R. Seresinhe, I. Staack, and C. Lawson, *Fuel consumption due to shaft power off-takes from the engine,* in *Proceedings of the 4th International Workshop on Aircraft System Technologies* (Aachen: Shaker, 2013).

[47] R. Bulirsch, J. Stoer, and J. Stoer, *Introduction to numerical analysis* (Springer, 1991).

[48] E. Torenbeek, *Synthesis of Subsonic Airplane Design: An introduction to the preliminary design of subsonic general aviation and transport aircraft, with emphasis on layout, aerodynamic design, propulsion and performance* (Springer Science & Business Media, 1982).

[49] Eaton Aerospace Limited, *Rear wing transfer pump, Data Sheet*, 8904 568-1-28708 (2013).

Appendix I - .json file for a PrP fuel system.

```
{
        "fuelGlobals": {
                "gen_freq": "cf",
                "jettison": "motor",
                "etops": false,
                "crossfeed": "rearWing1",
                "jet_setting": 2.0,
                "feed_route": ["rearWing", "verticalTail"],
                "transfer_routes": [["rearWing", "verticalTail", "
                   fuselageTransfer", "frontWing"], ["frontWing", "
                   fuselageTransfer", "fwdFuselage"]],
                "mounting_part": "fuselage"
        },

        "rearWing": {
                "wing_type": "tank",
                "spars": [0.3, 0.7],
                "rails": [0.15, 0.15],
                "locs": [[0, 0.7]],
                "filled": [0.3],
                "vent_box": [true, 0.05],
                "transfer_rail": "te",
                "rearWing1": {
                        "tank_type": "feed",
                        "jettison_loc": [0.15, 0.8],
                        "mirror": true,
                        "refuelling_station": false,
                        "transfer": {
                                "power": "motor",
                                "power_loc": [0.1, 0.8],
                                "valve_loc": [0.2, 0.8]
                        },
                        "feed_locs": {
                                "corner": "FI",
                                "wall_loc": [0.12, 0.3],
                                "span_locs": [0.3, 0.5, 0.7],
                                "chord_locs": [0.3, 0.3, 0.3]
                        },
                        "mirrored_parts": ["MotorPump", "TransferOutlet",
                           "Jettison", "CrossfeedBase", "FeedCell"]
                }
        },

        "frontWing": {
                "wing_type": "tank",
                "spars": [0.3, 0.7],
                "rails": [0.15, 0.15],
```

```
                "locs": [[0.09, 0.431], [0.5, 1]],
                "filled": [0.9, 0.9],
                "vent_box": [true, 0.05],
                "transfer_rail": "te",
                "frontWing1": {
                        "tank_type": "auxiliary",
                        "jettison_loc": [0.15, 0.8],
                        "mirror": true,
                        "refuelling_station": false,
                        "transfer": {
                                "power": "motor",
                                "power_loc": [0.1, 0.8],
                                "valve_loc": [0.2, 0.8]
                        },
                        "mirrored_parts": ["MotorPump", "TransferOutlet",
                           "Jettison"]
                },
                "frontWing2": {
                        "tank_type": "auxiliary",
                        "jettison_loc": [0.15, 0.5],
                        "mirror": true,
                        "refuelling_station": true,
                        "refuel_loc": [0.5, 0.2],
                        "transfer": {
                                "power": "motor",
                                "power_loc": [0.1, 0.8],
                                "valve_loc": [0.2, 0.8]
                        },
                        "mirrored_parts": ["MotorPump", "TransferOutlet",
                           "RefuelStation", "Jettison"]
                }
        },

        "verticalTail": {
                "wing_type": "passThrough",
                "spars": [0.2, 0.8],
                "rails": [0.05, 0.05],
                "transfer_rail": "te",
                "mirror": true
        },

        "connectingElement": {
                "wing_type": "None",
                "mirror": true
        },

        "fuselage": {
                "exitPoint": {
                        "exit_pt": [36.7819241, -2.53162567, 0],
                        "clearance": 0.2
                },
                "fwdFuselage": {
                        "tank_type": "auxiliary",
                        "mirror": false,
                        "vent_box": false,
                        "locs": [0, 0.015],
```

```
                        "fuselage_clearance": 0.2,
                        "floor_clearance": 0.2,
                        "bot_clearance": 0.3,
                        "tank_width": 0.7,
                        "rails": [[0.1, 0.2], [0.1, 0.2]],
                        "transfer_rail": "te",
                        "filled": [0.8],
                        "refuelling_station": false,
                        "jettison_loc": [0.3, 0.3],
                        "transfer": {
                                "power": "motor",
                                "power_loc": [0.6, 0.8],
                                "valve_loc": [0.2, 0.8]
                        }
                },
                "fuselageTransfer": {
                        "floor_clearance": 0.2,
                        "fuselage_clearance": 0.2,
                        "displacement": [0.1, -0.2],
                        "transfer_rail": "port",
                        "mirror": true
                }
        },

        "basin_cargo": {
                "tank_type": null,
                "mirror": false,
                "vent_box": false
        }
}
```